Received: 17 March 2022 | Revised: 17 September 2022 | Accepted: 11 November 2022

DOI: 10.1002/mma.8905

RESEARCH ARTICLE

WILEY

Edge detection from X-ray tomographic data for geometric image registration

Mohamed Lajili[1,2] | **Badreddine Rjaibi**[1] | **Didier Auroux**[3] | **Maher Moakher**[1]

[1]Laboratory for Mathematical and Numerical Modeling in Engineering Science, University of Tunis El Manar, National Engineering School at Tunis, Tunis-Belvedere, Tunisia

[2]Université de Haute-Alsace, Mulhouse, France

[3]Université Côte d'Azur,CNRS, LJAD, Nice, France

Correspondence
Maher Moakher, Laboratory for Mathematical and Numerical Modeling in Engineering Science, University of Tunis El Manar, National Engineering School at Tunis, B.P. 37, 1002 Tunis-Belvedere, Tunisia.
Email: maher.moakher@enit.utm.tn

Communicated by: N. Hyvonen

In this paper, we propose new variational model for image registration from tomographic data. First, we employ the topological gradient approach for a tomographic reconstruction that uses the first- and the second-order discontinuities in order to detect important objects of a given observed X-ray tomographic data (sinograms). Second, we use this geometric information furnished by a high-order operator in order to define an appropriate fidelity measure for the image registration process. A theoretical study of the proposed model is provided; Gauss–Newton method and multilevel technique are used for its numerical implementation. The performed numerical experiments show the efficiency and effectiveness of our model.

KEYWORDS

edge maps, fidelity measures, image registration, inverse problems, topological gradient, X-ray tomography

MSC CLASSIFICATION

65M32, 35Q68, 94A08, 65M22, 35G15

1 | INTRODUCTION

Image registration is a challenging image processing task that has applications in various fields like life sciences,[1] astronomy,[2] optics,[3] biology,[4] chemistry,[5] and remote sensing.[6] For instance, image registration is an important inverse problem in the domain of medical imaging. Indeed, usually a geometric deformation can occur during the steps of recording, reconstruction and transmission of images of the same object. Therefore, the images need to be geometrically aligned for better observation, especially in clinical diagnosis using medical images. The task of image registration is the determination of a geometrical transformation that aligns points in given image of an object with corresponding points in another image of that object. The two images could be different because they were taken at different times or were acquired using different devices like scanner, MRI, and CT. For details on image registration, the reader is referred to previous studies.[7–10] The image registration modeling can be illustrated by considering a pair of images: a given fixed image R called the reference and a moving image T called the template, both represented by scalar functions $R, T: \Omega \subset \mathbb{R}^2 \to \mathbb{R}$. The aim of image registration is to find a geometric transformation of the form $\varphi(\mathbf{x}) = \mathbf{x} + \mathbf{u}(\mathbf{x})$, where $\mathbf{u} : \mathbb{R}^2 \to \mathbb{R}^2$ is a displacement field such that aligns the two images, that is,

$$T[\varphi(\mathbf{x})] = T(\mathbf{x} + \mathbf{u}(\mathbf{x})) = R(\mathbf{x}). \tag{1}$$

In practice, the objective of image registration is to approximatively align the image T with the reference R by finding a reasonable deformation, in a way that the distance between R and a deformed version of T (registered image) is as small as possible. In parametric image registration, the type of the geometric transformation between these images is known a

prism and expressed by a finite number of parameters (e.g., translation and rotation). On the other hand, in the case of nonparametric image registration, the type of geometric transformation is unknown.

The reconstruction model (1) is an equation of the unknown displacement field $\mathbf{u}$, which is supposed to be sought in a properly chosen functional space. The model (1) is an ill-posed inverse problem and subsequently it is necessary to use regularization techniques. Generally, the regularization techniques turn an ill-posed problem into a well-posed problem. For this purpose, the problem (1) is reformulated as a minimization of an energy which is composed of two parts

$$\min_{\mathbf{u}\in(\mathcal{W}(\Omega,\mathbb{R}^2))} \{\phi\left(T(\mathbf{x}+\mathbf{u}(\mathbf{x}), R(\mathbf{x})\right) + \lambda J(\mathbf{u})\}, \tag{2}$$

where $\mathcal{W}(\Omega,\mathbb{R}^2)$ is a properly chosen functional space. The first part of the energy is a fidelity measure that quantifies similarity of the deformed version of $T(\mathbf{u})$ and the reference R. Indeed, the goal is to minimize (or to maximize) the term in which both images R and T are very similar. Generally, the choice of this term depends on the nature of images (monomodality and multimodality) to be registered. In the case of monomodal images, that is, the images are from the same modality (MRI T1, T2, and X-ray laser), have the same contrasts, and have similar features. Then, the preferred fidelity term of the energy (2) is often given by the "sum of squared differences" (SSD) or the "correlation coefficient" (CC) between $T(\mathbf{u})$ and R. Since these two terms make the registration between the pixels, then it is clear that such a measure only makes sense for monomodal images. For a pair of multimodal images, both images have different contrasts and the relation between the intensities of the two images is often much more complex. Various similarity measures have been used, such as "normalized gradient field" (see, e.g., previous studies[10–13]) and "the mutual information" (see, e.g., previous studies[10,14,15]).

The second part of the energy (2) is a regularization term which controls the smoothness of the displacement field $\mathbf{u}$ and reflects our expectations by penalizing unlikely transformations. From a mathematical point of view, the regularization term should turn the problem into a well-posed one, that is, leads to a unique minimizer and also if it is possible to a convex objective function. There are several regularizers that have been proposed until now, for example first-order derivatives which are based on total variation (see Hu et al.[16]) and diffusion (see Fischer and Modersitzki[17]) and higher order derivatives which are based on linear curvature.

In this paper, we are interested in deformable registration models from tomographic data. We suppose that the reference and the template images are given only by their tomographic measurements and should be simultaneously reconstructed and aligned. The idea, in this work, is to extract a geometric information (edges and thin structures) from tomographic data in a first step and use this information in a second step to build a robust and efficient similarity term. Indeed, in most registration models for multimodality images, the intensities of the same object in different images are not similar, but it is very often that the geometry (edges, gradient, and Hessian) is the same. Therefore, this geometric information is useful for defining a fidelity measure. As the gradient is described by first-order derivatives, it cannot detect discontinuity of second order, that is, discontinuity of the Laplacian/Hessian. However, this information may be valuable in clinical diagnosis using medical images and could be a very good indicative information for doctors. Moreover, the weakness of the gradient detection is also very sensitive to the noise that is always present in the images. To overcome these limitations, we use the topological gradient[18–22] of a high-order operator which is well suited for detecting discontinuities at different scales, that is, of first and second order. Believing in the elegance of deformable registration model from tomographic data, we aim to improve the image registration model for this case. This paper is organized as follows. In Section 2, we briefly discuss the modeling of the X-ray tomography problem. In Section 3, we give the formula of the topological gradient for the fourth-order model and display some examples which show the benefit of processing a fourth-order model. Section 4 is devoted to introducing our new variational model for image registration which is based on topological gradient and a theoretical analysis of the proposed model where we prove the existence of a solution. In Section 5, we present our numerical algorithm for topological gradient and image registration, and Section 6 displays numerical experiments. Brief conclusions are drawn in Section 7.

2 | THE X-RAY TOMOGRAPHY PROBLEM

The X-ray tomography problem might be considered as the restoration of an image inside the human body from a set of projections called sinogram which are X-ray line integrals of the processed image at some disposed direction. In our work, for the sake of simplicity, we focus on the case of parallel beam tomography when the directions of the X-ray are assumed

to be parallel. Mathematically, we can model the X-ray line integrals by the Radon transform operator[20] which is defined as follows:

$$R(f)(\theta, r) = \int_{\Omega} f(x, y)\delta(r - x\cos(\theta) - y\sin(\theta))dxdy,$$

where

- f is the processed image,
- Ω is an open-bounded convex domain of $\mathbb{R}^2$,
- θ and r are the polar coordinates of the X-ray direction, and
- $\delta(\cdot)$ is the Dirac punctual delta distribution.

For more information on the tomographic development and reconstruction approach, the reader is referred to previous studies.[18,20,21,23,24] In order to restore the image f, we must invert the Radon transform operator R. There are two ways to calculate the inversion formula for this problem.

- The first one is the analytic way based on the Fourier transform. The best one and the most used in this kind of inversion is the filtered back projection (FBP), it has a fast resolution algorithm, and it is efficient in the absence of high noise level. The idea of this algorithm is to filter the Fourier transforms of the projections in the variable r and then to apply the explicit inverted Radon transform at the filtered Fourier mode projections. To be precise we give the steps of this algorithm referred to on the famous Fourier slice theorem[20] as follows:

  1. Calculate the unidimensional Fourier transform $\widehat{F}_r$ of the projections with respect to the variable r:

  $$\widehat{F}_r R(f)(r, \theta).$$

  2. Filter the projections using a ramp filter:

  $$\tilde{f}(\rho, \theta) = \widehat{F}_r^{-1}|r|\widehat{F}_r R(f)(r, \theta),$$

  where $\widehat{F}_r^{-1}$ is the inverse Fourier transform with respect to the variable r.
  3. Restore the image f by applying the continuous back-projection transform R^* to $\tilde{f}$:

  $$f(x, y) = R^*\tilde{f}(\rho, \theta) = \int_0^{\pi} \tilde{f}(x\cos(\theta) + y\sin(\theta))d\theta.$$

- The algebraic formula is the second inversion way. It is based on the minimization over f of the following functional:

$$\|R(f) - g\|^2 + \lambda\phi(f), \tag{3}$$

where g is the sinogram data, λ is a regularization parameter, and ϕ is a regularization term. There are many ways to choose $\phi(f)$ (for more details, see previous studies[19,25,26]). In order to obtain a piecewise homogeneous image by preserving the majority of edges, the authors in previous studies[25–27] have shown that it is possible to consider $\phi(f) = \int_{\Omega}|\nabla f|^{\alpha}dxdy$ with $\alpha = 2$ in homogeneous parts and $\alpha = 1$ on the edges. The idea of this approach is to find edges with a fast and efficient optimization method, such as the topological gradient method,[28] and then to solve the following problem:

$$\begin{cases} -\mathrm{div}(\lambda(x)\nabla f) + R^*Rf = R^*g, & \text{in } \Omega, \\ \frac{\partial f}{\partial n} = 0, & \text{on } \partial\Omega, \end{cases} \tag{4}$$

with

$$\lambda(x) = \begin{cases} \frac{\lambda}{|\nabla f(x)|}, & \text{if } x \text{ belongs to the set of edges}, \\ \lambda, & \text{otherwise}, \end{cases} \tag{5}$$

and

$$R^*Rf = f * h, \text{ where } h(x, y) = \frac{1}{\sqrt{x^2 + y^2}}. \tag{6}$$

This approach is not fast as the FBP algorithm but is very efficient in the presence of high level of noise in the sinogram and there is a large choice to define an a priori regularization parameter λ that will produce a good image restoration result. Even though on the set of edges $|\nabla f|$ is not small, it is safer in the numerical implementation to replace the term $\frac{\lambda}{|\nabla f(x)|}$ in (5) by $\frac{\lambda}{\sqrt{|\nabla f(x)|^2+\epsilon}}$, where ϵ is a small threshold parameter.

3 | TOPOLOGICAL OPTIMIZATION TECHNIQUES FOR DETECTING GEOMETRIC INFORMATION FROM IMAGE

In this section, we study the problem of the detection of important features via the topological gradient method. In fact, there are two kinds of important features in the image: edges and thin structures. Every object in $(d-1)$-dimension can be linked to a structure that is assumed to be thin such as filaments in 3D or points in 2D. Generally, the derivation operator of first order detects edges, and it is not efficient to detect thin structures. There are some arguments to explain this:

- The intensity of the image is modified across the edges, which is not the case for thin structures.
- The two geometric structures do not have the same profile: Dirac delta form for thin structures and Heaviside form for edges.
- A thin structure is a very small and irregular object. In the presence of noise, it is very difficult to see it by a derivation operator of first order.

For the above reasons, some previous works[29–31] have proposed to use the operators of second order to identify thin structures. Fortunately, the topological gradient method provides an efficient optimization topological tool to detect this kind of geometric structures.[22,31]

The main idea of the topological gradient approach is to derive the following asymptotic expansion:

$$J_\epsilon(u_\epsilon) - J_0(u_0) = f(\epsilon)G(x_0) + o(f(\epsilon)), \tag{7}$$

where

- ϵ is a small positive parameter,
- J_ϵ (respectively, J_0) is a given cost function that defines the geometric structures of the image with respect to the parameter ϵ (respectively with respect to the initial domain Ω),
- u_ϵ (respectively, u_0) is a solution of the given PDE associated to tomographic problem on the perforated domain Ω_ϵ (respectively on the initial domain Ω),
- Ω is an open-bounded convex domain of $\mathbb{R}^2$,
- $\Omega_\epsilon = \Omega\backslash\overline{\omega_\epsilon}$, $\overline{\omega_\epsilon} = x_0 + \rho\omega$, $x_0 \in \Omega$, ω is a fixed cavity domain centered at the origin,
- $f(\epsilon)$ is a positive function tending to zero when ϵ goes to 0, and
- $G(x_0)$ is the topological gradient expression at x_0.

Generally, the choice of the cost function J_ϵ for the image restoration problem is based on the features of the geometric structures such as edges and thin structures. In order to preserve edges in the process of restoration the authors in previous studies[32–35] have used $J_\epsilon(u_\epsilon) = \int\limits_{\Omega_\epsilon} |\nabla u_\epsilon|^2 dx$, where $|\cdot|$ denotes the Euclidean norm in $\mathbb{R}^2$. In some other works, such as previous studies,[29–31] it has been shown that using the second-order derivative in the cost function is efficient to detect thin structures like points and filaments which are important information especially for the diagnostic of medical images. Recently, the authors in Houichet et al[22] have used the following cost function:

$$J_\epsilon(u_\epsilon) = \alpha \int\limits_{\Omega_\epsilon} |\Delta u_\epsilon|^2 dx + \beta \int\limits_{\Omega_\epsilon} |\nabla u_\epsilon|^2 dx,$$

where α and β are two positive parameters chosen by respecting the priority of the detection of edges or thin structures.

Auroux et al[27] have proposed to minimize the tomographic energy (3) outside the edges:

$$\int_{\Omega_\varepsilon} |R(u_\varepsilon) - g|^2 dx + \lambda \int_{\Omega_\varepsilon} |\nabla u_\varepsilon|^2 dx. \tag{8}$$

The Euler–Lagrange equation associated to this problem is

$$\begin{cases} -\mathrm{div}(\lambda \nabla u_\varepsilon) + R^* R u_\varepsilon = R^* g, & \text{in } \Omega_\varepsilon, \\ \frac{\partial u_\varepsilon}{\partial n} = 0, & \text{on } \partial\Omega_\varepsilon, \end{cases} \tag{9}$$

where $\vec{n}$ denotes the outside unit normal vector to $\partial\Omega_\varepsilon$.

They have obtained the following asymptotic expansion in the case where ω is a thin crack and $j(\varepsilon) = J_\varepsilon(u_\varepsilon) = \int_{\Omega_\varepsilon} |\nabla u_\varepsilon|^2 dx$:

$$j(\varepsilon) - j(0) = \varepsilon^2 G(x_0) + o(\varepsilon^2),$$

with

$$G(x_0) = -\pi\lambda(\nabla u_0(x_0)\cdot n)(\nabla v_0(x_0)\cdot n) - \pi|\nabla u_0(x_0)\cdot n|^2, \tag{10}$$

where v_0 is the solution of the adjoint problem

$$\begin{cases} -\mathrm{div}(\lambda \nabla v_0) + R^* R v_0 = 2\Delta u_0, & \text{in } \Omega, \\ \frac{\partial v_0}{\partial n} = 0, & \text{on } \partial\Omega. \end{cases} \tag{11}$$

In the present work, we propose to derive the asymptotic expansion defined in (7), by taking the following cost function:

$$J_\varepsilon(u_\varepsilon) = \int_\Omega \alpha_\varepsilon |\Delta u_\varepsilon|^2 dx + \int_\Omega \beta_\varepsilon |\nabla u_\varepsilon|^2 dx, \tag{12}$$

where

- $\alpha_\varepsilon = \begin{cases} \alpha_0, & \text{on } \Omega\backslash\overline{\omega_\varepsilon}, \\ \alpha_1, & \text{on } \omega_\varepsilon. \end{cases}$ and $\beta\varepsilon = \begin{cases} \beta_0, & \text{on } \Omega\backslash\overline{\omega_\varepsilon}, \\ \beta_1, & \text{on } \omega_\varepsilon. \end{cases}$
- $\omega_\varepsilon = x_0 + \varepsilon E$ and E is an ellipse whose boundary ∂E is defined by

$$\partial E = \{X(\theta) = (a\cos(\theta), b\sin(\theta)), 0 \le \theta \le 2\pi \text{ and } a, b > 0\}.$$

So the corresponding tomographic variational approach becomes

$$\min_{u_\varepsilon} \int_\Omega |R(u_\varepsilon) - g|^2 dx + \int_\Omega \alpha_\varepsilon |\Delta u_\varepsilon|^2 dx + \int_\Omega \beta_\varepsilon |\nabla u_\varepsilon|^2 dx. \tag{13}$$

The Euler–Lagrange equation associated to this problem is

$$\begin{cases} \Delta(\alpha_\varepsilon \Delta u_\varepsilon) - \mathrm{div}(\beta_\varepsilon \nabla u_\varepsilon) + R^* R u_\varepsilon = R^* g, & \text{in } \Omega, \\ \frac{\partial(\alpha_\varepsilon \Delta u_\varepsilon)}{\partial n} - \beta_\varepsilon \frac{\partial u_\varepsilon}{\partial n} = 0, & \text{on } \partial\Omega, \\ \Delta u_\varepsilon = 0, & \text{on } \partial\Omega. \end{cases} \tag{14}$$

In order to guarantee the existence and uniqueness of the solution u_ε, we propose to relax the problem (14) as follows:

$$\begin{cases} \Delta(\alpha_\varepsilon \Delta u_\varepsilon) - \operatorname{div}(\beta_\varepsilon \nabla u_\varepsilon) + R^* R u_\varepsilon + \mu u_\varepsilon = R^* g, & \text{in } \Omega, \\ \frac{\partial(\alpha_\varepsilon \Delta u_\varepsilon)}{\partial n} - \beta_\varepsilon \frac{\partial u_\varepsilon}{\partial n} = 0, & \text{on } \partial\Omega, \\ \Delta u_\varepsilon = 0, & \text{on } \partial\Omega, \end{cases} \tag{15}$$

where μ is a small positive parameter.

Lemma 1. *The corresponding variational formulation of problem (15) is given by*

$$\begin{cases} \text{Find } u_\varepsilon \in \mathcal{V} \text{ such that:} \\ a_\varepsilon(u_\varepsilon, v) = l_\varepsilon(v), \forall v \in \mathcal{V}, \end{cases} \tag{16}$$

where

- $a_\varepsilon(u_\varepsilon, v) = \int_\Omega \alpha_\varepsilon \Delta u_\varepsilon \Delta v dx + \int_\Omega \beta_\varepsilon \nabla u_\varepsilon \nabla v dx + \int_\Omega R^* R u_\varepsilon v dx + \int_\Omega \mu u_\varepsilon v dx,$
- $l_\varepsilon(v) = \int_\Omega R^* g v dx,$
- $\mathcal{V}$ *is the Hilbert space defined by*

$$\mathcal{V} = \{u_\varepsilon \in H^2(\Omega) \text{ such that } \Delta u_\varepsilon = 0 \text{ on } \partial\Omega\}.$$

Lemma 2. *For each $\varepsilon \geq 0$, the cost function J_ε is differentiable on $\mathcal{V}$ and its derivative is given by*

$$DJ_\varepsilon(u_0)(u_\varepsilon - u_0) = \int_\Omega 2\alpha_\varepsilon \Delta u_0 \Delta(u_\varepsilon - u_0) dx + 2 \int_\Omega \beta_\varepsilon \nabla u_0 \nabla(u_\varepsilon - u_0) dx. \tag{17}$$

Theorem 1. *There exist three real numbers δ_a, δ_l and δ_J that satisfy the following conditions:*

- $(a_\varepsilon - a_0)(u_0, v_\varepsilon) = \varepsilon^2 \delta_a + o(\varepsilon^2),$
- $(l_\varepsilon - l_0)(v_\varepsilon) = \varepsilon^2 \delta_l + o(\varepsilon^2),$
- $J_\varepsilon(u_\varepsilon) - J_0(u_0) = DJ_\varepsilon(u_0)(u_\varepsilon - u_0) + \varepsilon^2 \delta_J + o(\varepsilon^2),$

where v_ε is a solution of the adjoint problem

$$\begin{cases} \text{Find } v_\varepsilon \in \mathcal{V} \text{ such that:} \\ a_\varepsilon(w, v_\varepsilon) = -DJ_\varepsilon(u_0)w, \forall w \in \mathcal{V}. \end{cases} \tag{18}$$

In addition, we have

$$\begin{aligned} \delta_l &= 0, \\ \delta_J &= ab\pi \left[(\alpha_1 - \alpha_0)|\Delta u_0(x_0)|^2 + (\beta_1 - \beta_0)|\nabla u_0(x_0)|^2\right], \\ \delta_a &= ab\pi \left[(\alpha_1 - \alpha_0)\Delta u_0(x_0)\Delta v_0(x_0) + (\beta_1 - \beta_0)\nabla u_0(x_0)\nabla v_0(x_0)\right] \\ &\quad + (\alpha_0 - \alpha_1)(k_0^{a,b} + 1)\Delta v_0(x_0)\left(k_1^{a,b}\frac{\partial^2 u_0(x_0)}{\partial x^2} + k_2^{a,b}\frac{\partial^2 u_0(x_0)}{\partial y^2} + k_3^{a,b}\left(\frac{\partial^2 u_0(x_0)}{\partial x \partial y} + \frac{\partial^2 u_0(x_0)}{\partial y \partial x}\right)\right), \end{aligned}$$

where

$$k_0^{a,b} = \frac{2\pi}{2\int_0^{\frac{\pi}{2}} \sqrt{a^2\cos^2(\theta) + b^2\sin^2(\theta)}d\theta - \pi},$$
$$k_1^{a,b} = \int_0^{2\pi} \frac{a^2\cos^2(\theta)}{\sqrt{a^2\cos^2(\theta) + b^2\sin^2(\theta)}}d\theta,$$
$$k_2^{a,b} = \int_0^{2\pi} \frac{b^2\sin^2(\theta)}{\sqrt{a^2\cos^2(\theta) + b^2\sin^2(\theta)}}d\theta,$$
$$k_3^{a,b} = \int_0^{2\pi} \frac{ab\cos(\theta)\sin(\theta)}{\sqrt{a^2\cos^2(\theta) + b^2\sin^2(\theta)}}d\theta.$$

The proof of existence of the three numbers δ_a, δ_l, and δ_J is given in Appendix A.

Theorem 2. *The topological gradient expression associated to the cost function defined by (12) where u_ε is the solution of the problem (13) is given by*

$$\begin{aligned} g(x_0) &= \delta_a - \delta_l + \delta_J, \\ &= ab\pi\left[(\alpha_1 - \alpha_0)|\Delta u_0(x_0)|^2 + (\beta_1 - \beta_0)|\nabla u_0(x_0)|^2\right] \\ &\quad + ab\pi\left[(\alpha_1 - \alpha_0)\Delta u_0(x_0)\Delta v_0(x_0) + (\beta_1 - \beta_0)\nabla u_0(x_0)\nabla v_0(x_0)\right] \\ &\quad + (\alpha_0 - \alpha_1)(k_0^{a,b} + 1)\Delta v_0(x_0)\left(k_1^{a,b}\frac{\partial^2 u_0(x_0)}{\partial x^2} + k_2^{a,b}\frac{\partial^2 u_0(x_0)}{\partial y^2} + k_3^{a,b}\left(\frac{\partial^2 u_0(x_0)}{\partial x\partial y} + \frac{\partial^2 u_0(x_0)}{\partial y\partial x}\right)\right), \end{aligned} \tag{19}$$

where u_0 (respectively, v_0) is the solution of problem (13) with $\varepsilon = 0$ (respectively, problem A1).

Proof. From the third assertion of Theorem 1, we have

$$J_\varepsilon(u_\varepsilon) - J_0(u_0) = DJ_\varepsilon(u_0)(u_\varepsilon - u_0) + \varepsilon^2\delta_J + o(\varepsilon^2).$$

According to Equation (18), we get

$$\begin{aligned} J_\varepsilon(u_\varepsilon) - J_0(u_0) &= -a_\varepsilon(u_\varepsilon - u_0, v_\varepsilon) + \varepsilon^2\delta_J + o(\varepsilon^2), \\ &= -a_\varepsilon(u_\varepsilon, v_\varepsilon) + a_\varepsilon(u_0, v_\varepsilon) + \varepsilon^2\delta_J + o(\varepsilon^2), \\ &= -a_\varepsilon(u_\varepsilon, v_\varepsilon) + a_0(u_0, v_\varepsilon) - a_0(u_0, v_\varepsilon) + a_\varepsilon(u_0, v_\varepsilon) + \varepsilon^2\delta_J + o(\varepsilon^2), \\ &= (a_\varepsilon - a_0)(u_0, v_\varepsilon) + (l_0 - l_\varepsilon)(v_\varepsilon) + \varepsilon^2\delta_J + o(\varepsilon^2). \end{aligned}$$

Then, according to the first and second assertions of Theorem 1, we deduce that

$$J_\varepsilon(u_\varepsilon) - J_0(u_0) = (\delta_a - \delta_l + \delta_J)\varepsilon^2 + o(\varepsilon^2).$$

□

The result of the previous theorem is proved for a particular case of an ellipse centered at x_0 whose parametric equations are as follows:

$$\begin{cases} x_1 = a\cos(\theta), \\ x_2 = b\sin(\theta), \end{cases}$$

for all $\theta \in [0, 2\pi[$. When we take $a = 1$ and send b to zero, we deduce the expression of the topological gradient in the case of a crack:

$$g(x_0) = 4(\alpha_0 - \alpha_1)\left(\frac{\pi + 2}{2 - \pi}\right)\Delta v_0(x_0)\frac{\partial^2 u_0(x_0)}{\partial x^2}. \tag{20}$$

3.1 | The benefit of using the topological gradient of a high-order operator

It is clear that when $\alpha_\varepsilon = 0$, the above tomographic variational approach (13) corresponds to the well-known minimization problem (8) which uses only first-order derivatives of an input image. In this case, the high-order topological gradient (20), that we have found, becomes an operator which is expressed by only first-order derivative given by (10). This has disadvantage when, for example, the image contains a very sensitive geometrical information such as thin structures (points and filaments) which are not detectable by first-order derivatives. In order to show the efficiency of the proposed topological gradient approach in detecting thin structures, we tested the proposed model for $\alpha_\varepsilon = 0$ and $\alpha_\varepsilon \neq 0$ for edge detection. In Figure 1, we have three examples of images that contain thin structures. In Figure 1A, we assess the performance of the second-order T-G in detecting thin structures such as blood vessels and veins. In Figure 1B, we have a synthetic image described by a very sensitive geometrical information. In Figure 1C, we show the efficiency of the second-order derivative for medical images. It is clear the map α_ε is unable to detect the gradient discontinuities. Then, the second-order topological gradient is more efficient than the first-order topological gradient in detecting thin structures. These results highlight the importance of the high-order terms in detecting and preserving thin structures.

4 | THE PROPOSED MONOMODALITY/MULTIMODALITY MODEL

In this section, we propose a new registration model for monomodality/multimodality images. This approach is based on geometric information which is detected by one of the best topological optimization tools: the topological gradient method (T-G). Let $S_R, S_T: \Omega \subseteq \mathbb{R}^2 \to \mathbb{R}$ be two given observed X-ray tomographic data (sinograms), where the first is

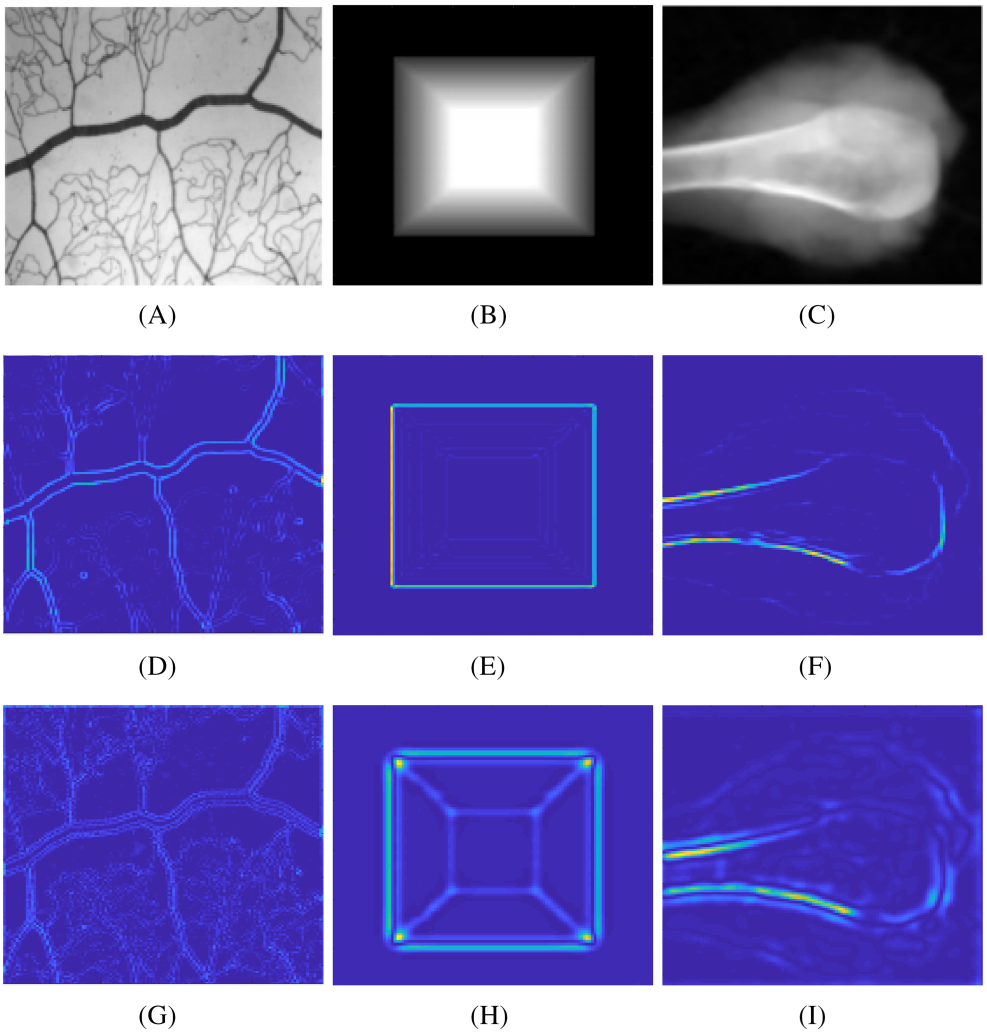

FIGURE 1 Example of geometric information which are detected by the T-G of first and second order. (A–C) Original images. (D–F) The map of β_ε: topological gradient for the second-order model ($\alpha_\varepsilon = 0$). (G–I) The map of α_ε: topological gradient for the fourth-order model [Colour figure can be viewed at wileyonlinelibrary.com]

called sinogram of the reference image and the second is called sinogram of the template image. In order to align the template image with the reference one, we propose the following steps:

First, we detect the edges and thin structures for both images from X-ray tomographic data using the topological gradient method. Then, we use this geometric information which is obtained by the topological gradient in order to define a fidelity measure in the image registration process.

Second, we choose the fidelity measure which is based on the geometric structures that are detected from both images S_R and S_T, as follows:

$$\phi\left(T(\mathbf{x}+\mathbf{u}(\mathbf{x}), R(\mathbf{x})\right) = \frac{1}{2}\|TG(\mathbf{u}) - RG\|_2^2,$$

where RG (respectively, TG) is the set of edges and thin structures that are detected from X-ray tomographic data S_R (respectively, S_T) by the T-G method.

However, for the choice of the regularizer term, there is a large set of regularizer terms that have been used in previous works. This lead us to ask how to choose the best regularization term that gives the more possible plausible transformation. In this work, we choose a robust regularizer that allows a large smoothness outside the discontinuities, which is composed of both first- and second-order derivatives (gradient and Hessian) of the deformation field $\mathbf{u}$ as follows:

$$J(\mathbf{u}) = \frac{\lambda}{2}\int_\Omega |\nabla \mathbf{u}|^2 dx + \frac{\alpha}{2}\int_\Omega |\nabla^2 \mathbf{u}|^2 dx.$$

Based on these two choices, we propose to register the two functions S_R, S_T by solving the following minimization problem:

$$\min_{\mathbf{u}\in\mathcal{W}}\left\{\mathcal{J}(\mathbf{u}) = \frac{1}{2}\|TG(\mathbf{u}) - RG\|_2^2 + \frac{\lambda}{2}\int_\Omega |\nabla \mathbf{u}|^2 dx + \frac{\alpha}{2}\int_\Omega |\nabla^2 \mathbf{u}|^2 dx\right\}, \tag{21}$$

where λ and α are regularization parameters, and

$$\mathcal{W} = \left\{\mathbf{u} \in \mathcal{W}_0^{1,2}(\Omega) \cap \mathcal{W}^{2,2}(\Omega) \text{ such that } \frac{\partial \mathbf{u}}{\partial n} = 0 \text{ on } \partial\Omega\right\}.$$

For the choice of two successive regularization parameters, the challenge is how to choose the good parameters which give the best diffeomorphic registration and hence the choice of a good one becomes delicate. In Figure 2, we show the key role played by the choice of the parameters on the efficiency of regularization. In Figure 2G–J, it is clear that the energy (21) is unable to minimize the dissimilarity between R and T. In Figure 2K,L, we assess that the variational method (21) is efficient in ensuring that the obtained transformation corresponds to a plausible deformation. These results highlight the importance of the regularization parameters in controlling the characteristics of the deformation (Figure 2H,J,L).

In the remainder of this section, we focus on the mathematical study of the proposed model. Our goal is to prove that problem (21) has at least one solution in the space $\mathcal{W}$. The energy $\mathcal{J}(\mathbf{u})$ is nonconvex with respect to $\mathbf{u}$, and consequently, the proof of the weak lower semicontinuity is not straightforward. For that, we will use the concept of Carathéodory functions defined in Theljani and Chen[10] as follows:

Definition 1. Let $\Omega \subset \mathbb{R}^d$ be an open set and let $f : \Omega \times \mathbb{R}^n \times \mathbb{R}^{d\times n} \times \mathbb{R}^{d\times d\times n} \to [0, +\infty]$ satisfies the following assumptions:

- $f(x, \cdot, \cdot, \cdot)$ is continuous for almost every $x \in \Omega$,
- $f(x, \mathbf{u}, \phi, \theta)$ is measurable in x for every $(\mathbf{u}, \phi, \theta) \in \mathbb{R}^n \times \mathbb{R}^{d\times n} \times \mathbb{R}^{d\times d\times n}$.

Then, f is a Carathéodory function.

Definition 2. Let $f : I \to \mathbb{R}$, where I is a convex set. Then, f is a quasiconvex function if

$$\forall (x, y) \in I^2, \forall \lambda \in [0, 1], f(\lambda x + (1-\lambda)y) \le \max\{f(x), f(y)\}.$$

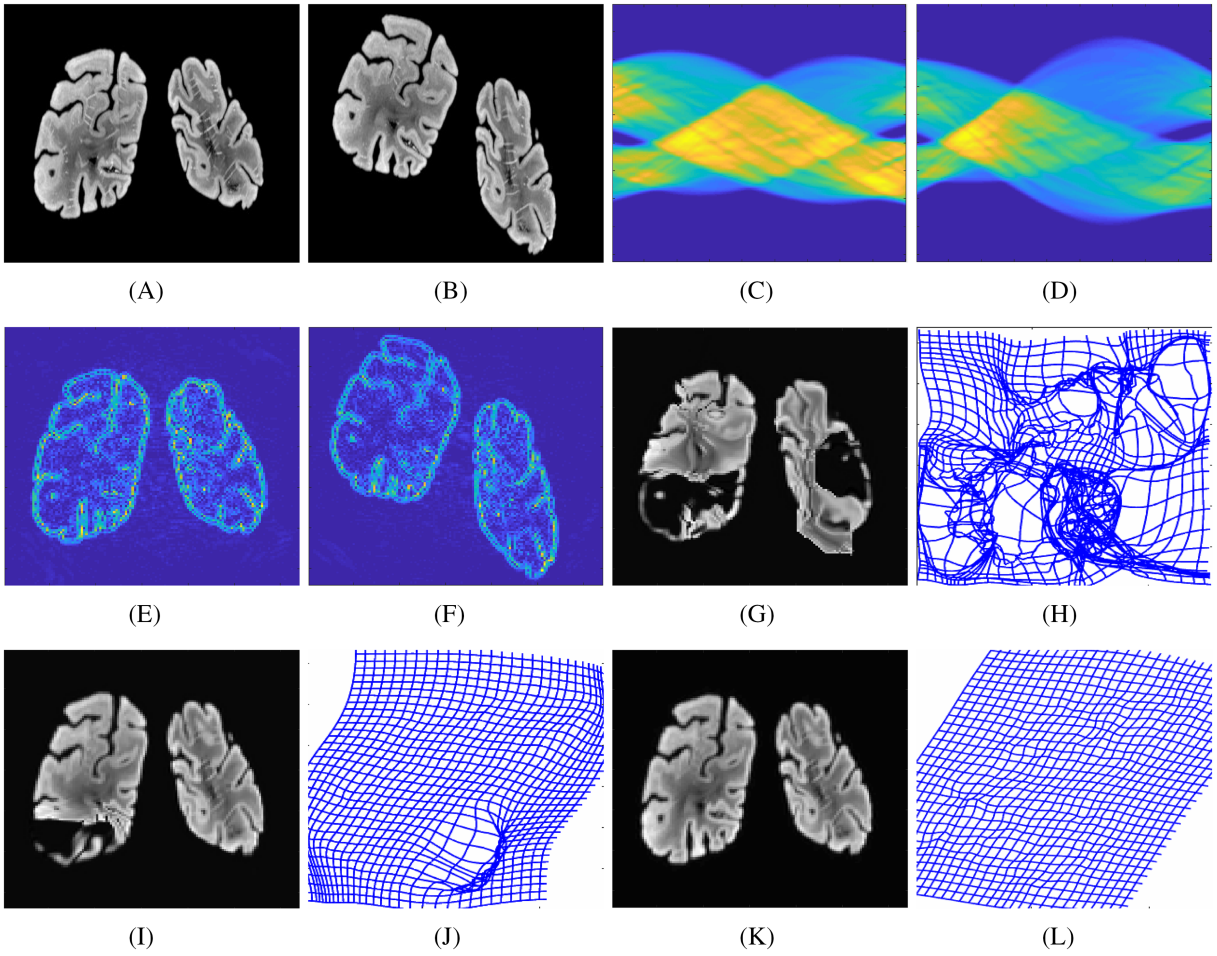

FIGURE 2 Example of image registration results for monomodal image registration by using our model. This figure illustrates the key role of the choice of the regularization parameters. (A) R: corresponding image for S_R. (B) T: corresponding image for S_T. (C) Reference sinogram S_R. (D) Template sinogram S_T. (E) RG: geometric information for S_R. (F) TG: geometric information for S_T. We tested the minimization problem (21) with (G,H) $\lambda = 10$ and $\alpha = 20$ or (I,J) $\lambda = 150$ and $\alpha = 100$ or (K,L) $\lambda = 1000$ and $\alpha = 1000$. The deformation is recovered by image registration, resulting in the images (G), (I), and (K) [Colour figure can be viewed at wileyonlinelibrary.com]

Now, we will start by giving some assumption and lemmas which are needed to prove that our optimization problem admits a minimizer.

We will assume that

- The fixed image RG and the moving image TG are continuous.
- $|TG(\mathbf{u})|$ and $|RG|$ are bounded almost everywhere by a constant $c > 0$.

Lemma 3 (Theljani and Chen[10]). *Let $\Omega \subset \mathbb{R}^d$ be an open set and $f : \Omega \times \mathbb{R}^n \times \mathbb{R}^{d\times n} \times \mathbb{R}^{d\times d\times n} \to [0, +\infty]$. Then, $\mathcal{J}(\boldsymbol{u}) = \int_\Omega f(x, \boldsymbol{u}, \phi, \theta)dx$ is weakly lower semicontinuous in $\mathcal{W}$ if*

- *f is a Carathéodory function,*
- *$f(x, \boldsymbol{u}, \phi, \theta)$ is quasiconvex with respect to θ,*
- *$0 \le f(x, \boldsymbol{u}, \phi, \theta) \le a(x) + C(|\phi|^p + |\theta|^p)$ where $a(x) \in L^1(\Omega)$ and $C > 0$.*

Lemma 4. *Let $\mathcal{J}(\cdot)$ be the energy functional defined in $\mathcal{W}$ by*

$$\mathcal{J}(\boldsymbol{u}) = \int_\Omega f(x, \boldsymbol{u}, \nabla\boldsymbol{u}, \nabla^2\boldsymbol{u})dx, \tag{22}$$

where

$$f(x, \boldsymbol{u}, \nabla \boldsymbol{u}, \nabla^2 \boldsymbol{u}) = \frac{1}{2}|TG(\boldsymbol{u}) - RG|^2 + \frac{\lambda}{2}|\nabla \boldsymbol{u}|^2 + \frac{\alpha}{2}|\nabla^2 \boldsymbol{u}|^2. \tag{23}$$

Then, $\mathcal{J}(\cdot)$ is coercive and weakly lower semicontinuous (wlsc) in $\mathcal{W}$.

Proof. We have

$$\mathcal{J}(\mathbf{u}) = \int_\Omega \left(\frac{1}{2}|TG(\mathbf{u}) - RG|^2 + \frac{\lambda}{2}|\nabla \mathbf{u}|^2 + \frac{\alpha}{2}|\nabla^2 \mathbf{u}|^2\right) dx.$$

Using the positivity of $\int_\Omega \frac{1}{2}|TG(\mathbf{u}) - RG|^2 dx$, we obtain

$$\mathcal{J}(\mathbf{u}) \geq \frac{\min(\lambda, \alpha)}{2} \int_\Omega |\nabla \mathbf{u}|^2 + |\nabla^2 \mathbf{u}|^2 dx.$$

By using Poincaré's inequality, we show that

$$\|\mathbf{u}\|_{\mathcal{W}} = \left(\|\nabla \mathbf{u}\|_2^2 + \|\nabla^2 \mathbf{u}\|_2^2\right)^{\frac{1}{2}}$$

is a norm on the space $\mathcal{W}$. Thus, we obtain

$$\mathcal{J}(\mathbf{u}) \geq \frac{1}{2} \min(\lambda, \alpha) \|\mathbf{u}\|_{\mathcal{W}}^2.$$

which directly gives the coercivity of $\mathcal{J}(\cdot)$.

For the wlsc of $\mathcal{J}(\cdot)$, we now check that the function $f(\cdot)$ fulfills the assumptions in Lemma 3. Since the images RG and TG are assumed continuous almost everywhere on their domain then $f(\cdot)$ is Carathéodory function. In addition, it is easy to check that $f(x, \mathbf{u}, \nabla \mathbf{u}, \nabla^2 \mathbf{u})$ is convex with respect to $\nabla^2 \mathbf{u}$, clearly implying that it is quasiconvex. Moreover, as we have assumed earlier that $|TG(\mathbf{u})|$ and $|RG|$ are bounded almost everywhere by a constant $c > 0$, we deduce that

$$\frac{1}{2}|TG(\mathbf{u}) - RG|^2 \leq \frac{1}{2}(|TG(\mathbf{u})| + |RG|)^2 \leq 2c^2.$$

Then, we get

$$0 \leq f(x, \mathbf{u}, \nabla \mathbf{u}, \nabla^2 \mathbf{u}) = \frac{1}{2}|TG(\mathbf{u}) - RG|^2 + \frac{\lambda}{2}|\nabla \mathbf{u}|^2 + \frac{\alpha}{2}|\nabla^2 \mathbf{u}|^2,$$

which implies

$$0 \leq f(x, \mathbf{u}, \nabla \mathbf{u}, \nabla^2 \mathbf{u}) \leq 2c^2 + \frac{\lambda}{2}|\nabla \mathbf{u}|^2 + \frac{\alpha}{2}|\nabla^2 \mathbf{u}|^2.$$

Consequently, the function $f(\cdot)$ fulfills the third condition of Lemma 3 with $a(x) = 2c^2 \in L^1(\Omega)$ and $C = \frac{1}{2}\max(\lambda, \alpha)$. Finally, we deduce that the energy $\mathcal{J}(\cdot)$ is weakly lower semicontinuous in $\mathcal{W}$. □

Theorem 3. *The minimization problem (21) admits at least one solution in the space $\mathcal{W}$.*

Proof. Let $(\mathbf{u}_n)_{n\in\mathbb{N}} \subset \mathcal{W}$ of $\mathcal{J}(\cdot)$ be a minimizing sequence, that is,

$$\mathcal{J}(\mathbf{u}_n) \underset{n\to+\infty}{\longrightarrow} \min_{\mathbf{u}\in\mathcal{W}} \mathcal{J}(\mathbf{u}).$$

The coercivity of $\mathcal{J}(\cdot)$ implies that $(\mathbf{u}_n)_{n\in\mathbb{N}}$ is uniformly bounded in $\mathcal{W}$. Thus, the boundedness of $(\mathbf{u}_n)_{n\in\mathbb{N}}$ guarantees the existence of a subsequence, still denoted $(\mathbf{u}_n)_{n\in\mathbb{N}}$ such that $\mathbf{u}_n \underset{n\to+\infty}{\rightharpoonup} \mathbf{u}$ in $\mathcal{W}$. By using the wlsc of $\mathcal{J}(\cdot)$ proved in Lemma 3, i.e., $\mathcal{J}(\mathbf{u}) \leq \lim_{n\to+\infty} \mathcal{J}(\mathbf{u}_n) = \min_{\mathbf{u}\in\mathcal{W}} \mathcal{J}(\mathbf{u})$, we show that the limit $\mathbf{u}$ is a minimizer of $\mathcal{J}(\cdot)$. □

5 | NUMERICAL EXPERIMENTS

The goal of this section is to prove that topological gradient approach of a high-order operator is able to define a fidelity measure for image registration. First, we give an algorithm that consists of inserting small cracks in regions where the topological gradient $g(x_0)$ is smaller than a given threshold $\xi < 0$. These regions represent the geometric information (edges, thin structures) of the image. Then, we give the Gauss–Newton algorithm which is well adapted for a nonlinear least squares optimization problem. Finally, we give the multilevel image registration algorithm.

5.1 | Step 1: Geometric information from the tomographic data

Before going to the numerical study of problem (A2), let us remind the algorithm of the topological gradient for detecting geometric information from image (i.e., how to obtain TG and RG).

In this algorithm, we have to solve one direct and one adjoint PDE problem in order to calculate the topological gradient expression. These problems are linear which leads to obtain a linear system: $Ax = B$ based on the finite element method. This provided the operator R^*R is assembled. Where R is the system matrix defining the discrete Radon operator, defined by

$$R(i,j) = \begin{cases} 1 & \text{if the projection } i \text{ crosses the position } j \text{ of the object,} \\ 0 & \text{otherwise,} \end{cases}$$

and R^* is the dual discrete operator of R ($R^* = R$). According to the properties of the operators defined in the direct and adjoint PDE problem, we show that A is a positive definite symmetric matrix. For the computational cost of the topological gradient method, we solve this linear system with a preconditioned conjugate gradient method which requires $O(n^2 log(n))$ operations for an object with $n \times n$ pixels.

Algorithm 1 T-G's approach to the reconstruction of the image and detection of its geometric information.

- Initalization: $\lambda = \lambda_0,\ \alpha_\varepsilon = \alpha_0$ and $\beta_\varepsilon = \beta_0$.

A. Edges detection:
- Calculation of u_0 and v_0 by solving the direct (9) and the adjoint (11) problems.
- Determination of the edges set I_1 defined by

$$I_1 = \{x_0 \in \Omega \text{ such that } G(x_0) < \xi_1 < 0\},$$

where ξ_1 is a given negative threshold and $G(x_0)$ is the topological gradient defined in (10) .

B. Thin structures detection:
- Calculation of u_0 and v_0 by solving the direct (15) and the adjoint (18) problems.
- Calculation of the topological gradient (10) for detecting edges.
- Determination of the thin structures set I_2 defined by

$$I_2 = \{x_0 \in \Omega \text{ such that } g(x_0) < \xi_2 < 0\},$$

where ξ_2 is a given negative threshold and $g(x_0)$ is the topological gradient defined in (20).

C. Geometric structures information:
- The geometric structures information is defined by the following set:

$$\omega = I_1 \cup I_2$$

5.2 | Step 2: Image registration process

5.2.1 | Gauss–Newton method

Our model is a highly nonlinear least squares problem, and its numerical solution is a nontrivial task. For this purpose, we propose a Gauss–Newton method for solving the minimization problem by replacing the original nonlinear system with a linear one. Indeed, the Gauss–Newton scheme is as follows: Starting from an initial guess δU, we compute the gradient $G_{\mathcal{J}}$ at each step. Then, we improve this guess by an update δU which is solution of the linear system:

$$\mathcal{H}\delta U = -G_{\mathcal{J}}. \tag{24}$$

The process is repeated until convergence, that is, $\|\delta U - \delta U_{old}\| \leq \varepsilon$, where ε is a given threshold. We note that $\mathcal{H}$ is an approximated Hessian which is symmetric and positive definite.

In order to obtain the descretization formulation for the model (21), we use finite differences on a unit square domain $\Omega =]0,1[^2$. In implementation, we employ a nodal grid and define a discretized square domain by the uniform grid

$$\left\{\mathbf{x}^{i,j} = (x_1^i, x_2^j) = (ih, jh),\ 0 \leq i, j \leq n\right\},$$

where $h = \frac{1}{n}$. We discretize the uniform displacement field $\mathbf{u}$ on the nodal grid $\mathbf{x}^{i,j}$ and $\mathbf{u}^{i,j}$, namely, $\mathbf{u}^{i,j} = (u_1^{i,j}, u_2^{i,j}) = (u_1(x_1^i, x_2^j), u_2(x_1^i, x_2^j))$. According to the lexicographical ordering, we reshape the matrices into two long vectors of dimension $\mathbb{R}^{2(n+1)^2 \times 1}$. Then, we approximate the first-order and second-order regularization terms by using the forward difference, central difference, mid-point rule, and Dirichlet boundary conditions. For more information and details, the reader is referred to Lajili et al[36] and Zhang et al.[37]

Algorithm 2 Gauss–Newton method by using Armijo line search for image registration: $U \leftarrow \text{GNIR}(U_0)$.

Start with an initial guess $U \longleftarrow U_0$;
While not converged **do**

1. Evaluate $\mathcal{J}$, $G_{\mathcal{J}}$ and $\mathcal{H}$ at U
2. Solve the descent direction from the linear equation $\mathcal{H}\delta U = -G_{\mathcal{J}}$
3. Find a positive scalar step-size s using line search scheme
4. Update $U \longleftarrow U + s\delta U$

end

5.2.2 | Multilevel technique

A major difficulty in numerical optimization is the nonconvexity of the model. Constructing a numerical optimization algorithm that avoids being trapped in a local minimum is very important for solving a nonconvex model. Here, we

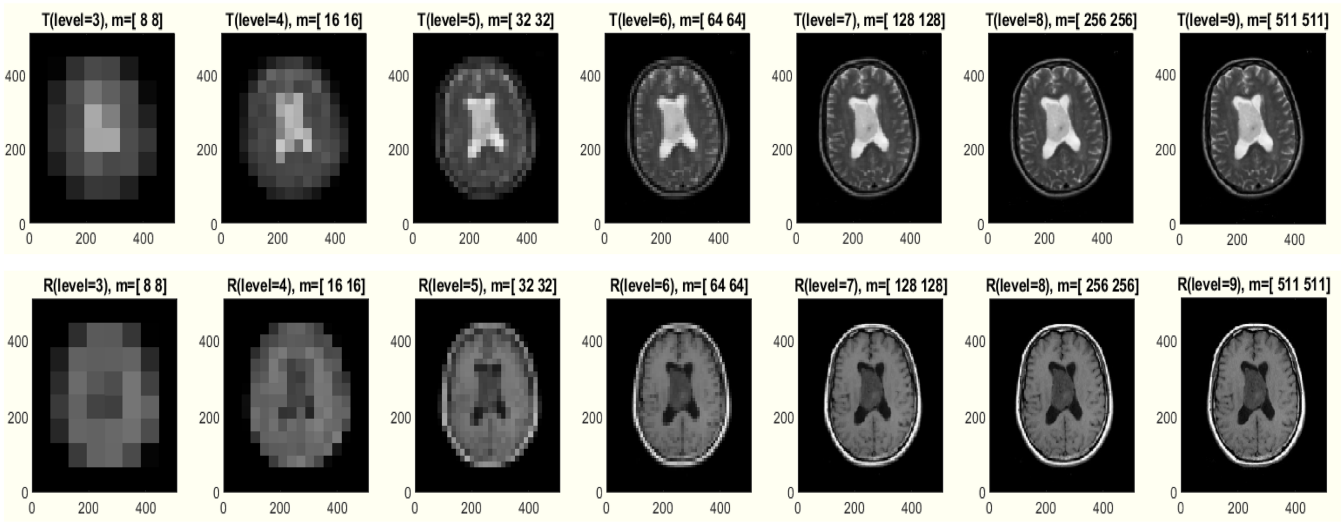

FIGURE 3 Example of a multilevel representation of both images R and T of size 511×511 [Colour figure can be viewed at wileyonlinelibrary.com]

TABLE 1 Run times for the image registration process

Figure	4	5	6	7	9	10
Time (s)	13.617	12.173	10.384	11.907	13.094	12.957

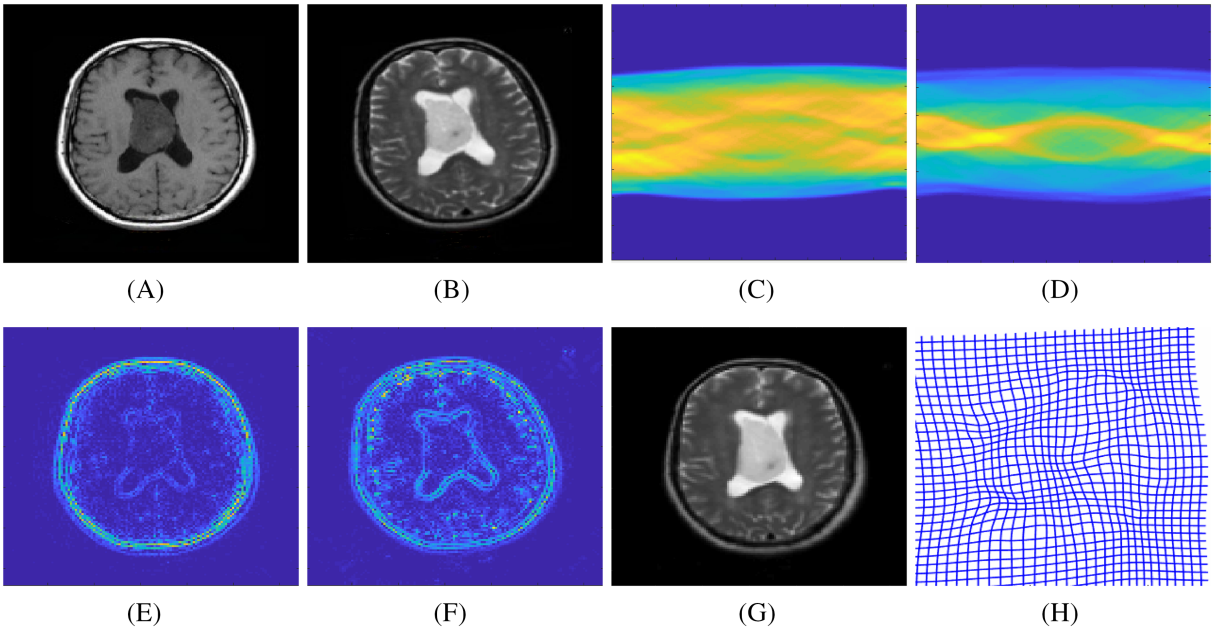

FIGURE 4 Example of a nonparametric multimodal image registration by using our model. (A) R: corresponding image for S_R. (B) T: corresponding image for S_T. (C) Reference sinogram S_R. (D) Template sinogram S_T. (E) RG: geometric information for S_R. (F) TG: geometric information for S_T. (G) Registered image $T(\varphi)$, $\mathcal{E}_r = 0.48$. (H) The deformation $\varphi(x) = x + \mathbf{u}(x)$ [Colour figure can be viewed at wileyonlinelibrary.com]

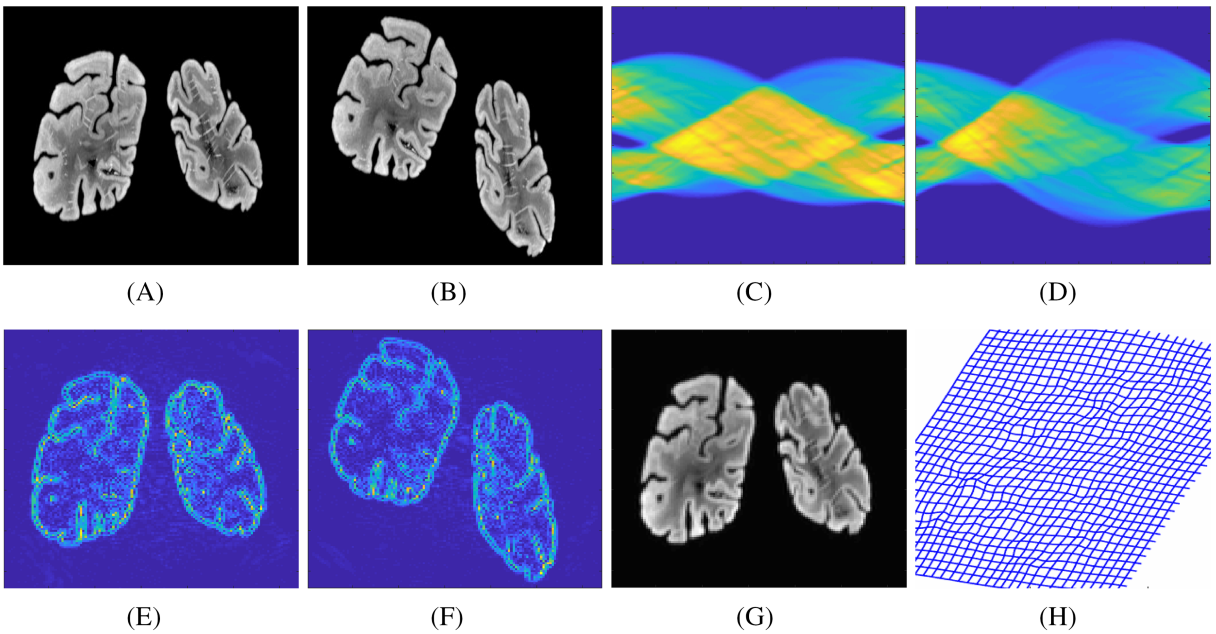

FIGURE 5 Example of a monomodal image registration by using our model. (A) R: corresponding image for S_R. (B) T: corresponding image for S_T. (C) Reference sinogram S_R. (D) Template sinogram S_T. (e) RG: geometric information for S_R. (F) TG: geometric information for S_T. (G) Registered image $T(\varphi)$, $\mathcal{E}_r = 0.08$. (H) The deformation $\varphi(x) = x + \mathbf{u}(x)$ [Colour figure can be viewed at wileyonlinelibrary.com]

overcome these limitations by a multilevel technique, which assures the numerical solution serves as a perfect starting point and speeds up the registration process. Indeed, starting with the initial guess $U = 0$, the idea is to improve this guess by resizing the original images to a sequence of coarser ones where computations are cheap and register these smaller images (see Figure 3). Then, starting from the coarsest level, we interpolate the update U to get a starting guess on next levels until the original resolution on the finest level is reached.

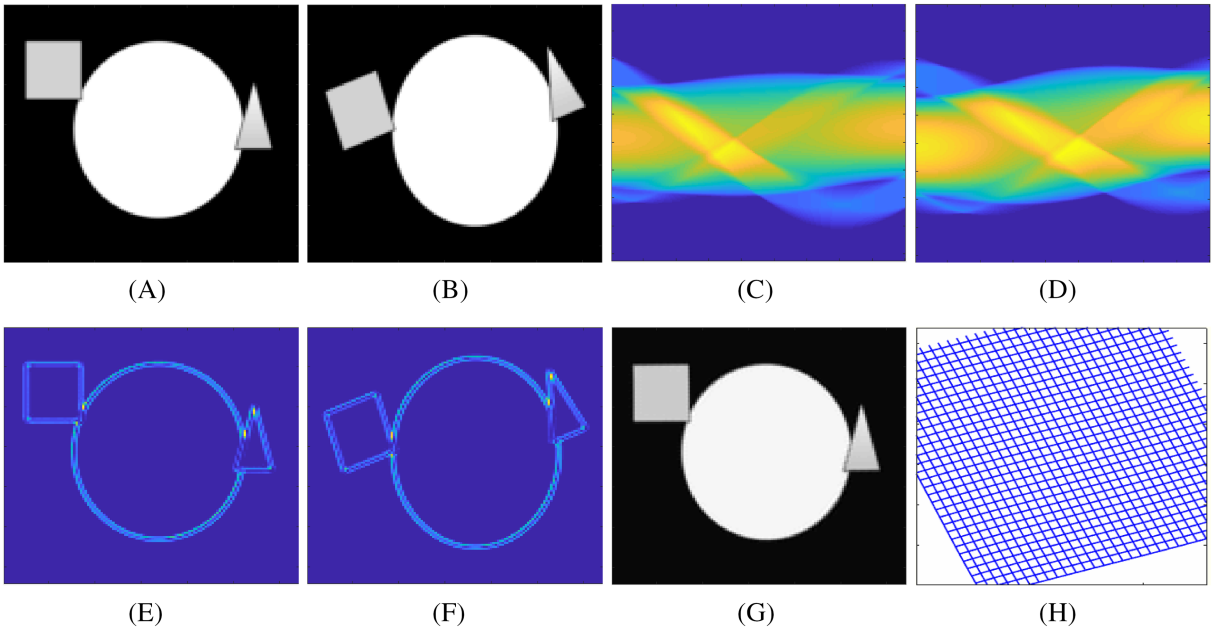

FIGURE 6 Example of a parametric monomodal image registration by using our model. The geometric transformation between the reference and the template images is in the form of a 30° rotation. (A) R: corresponding image for S_R. (B) T: corresponding image for S_T. (C) Reference sinogram S_R. (D) Template sinogram S_T. (E) RG: geometric information for S_R. (F) TG: geometric information for S_T. (G) Registered image $T(\varphi)$, $\mathcal{E}_r = 0.04$. (H) The deformation $\varphi(x) = x + \mathbf{u}(x)$ [Colour figure can be viewed at wileyonlinelibrary.com]

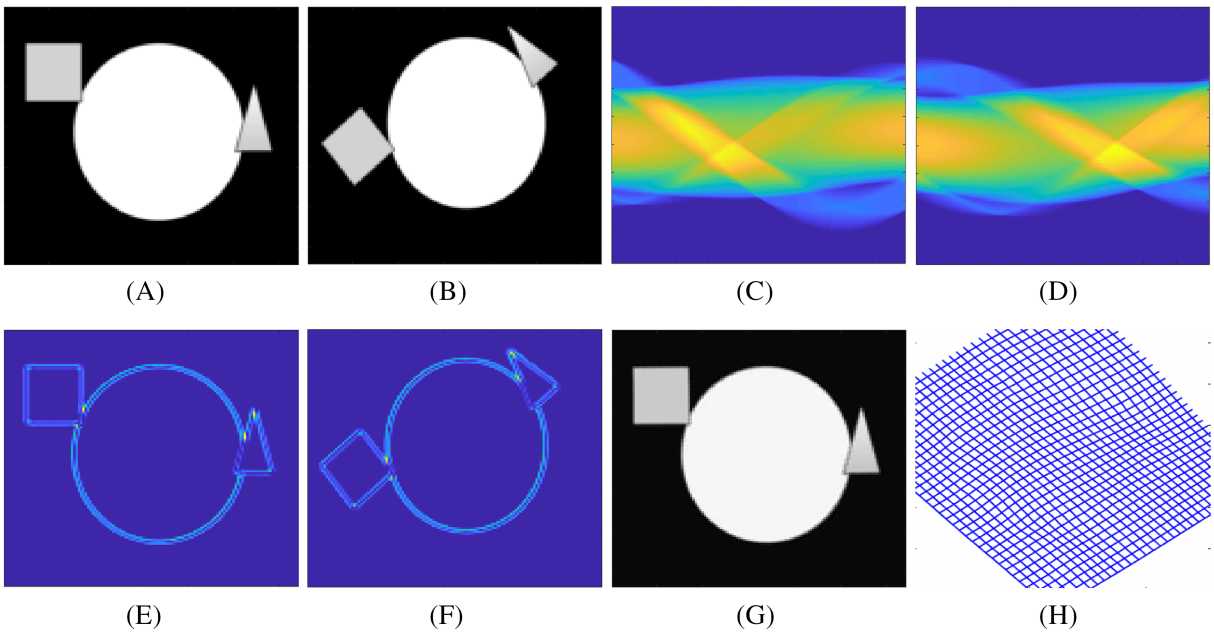

FIGURE 7 Example of a parametric monomodal image registration by using our model. The geometric transformation between the reference and the template images is in the form of a 45° rotation. (A) R: corresponding image for S_R. (B) T: corresponding image for S_T. (C) Reference sinogram S_R. (D) Template sinogram S_T. (E) RG: geometric information for S_R. (F) TG: geometric information for S_T. (G) Registered image $T(\varphi)$, $\mathcal{E}_r = 0.09$. (H) The deformation $\varphi(x) = x + \mathbf{u}(x)$ [Colour figure can be viewed at wileyonlinelibrary.com]

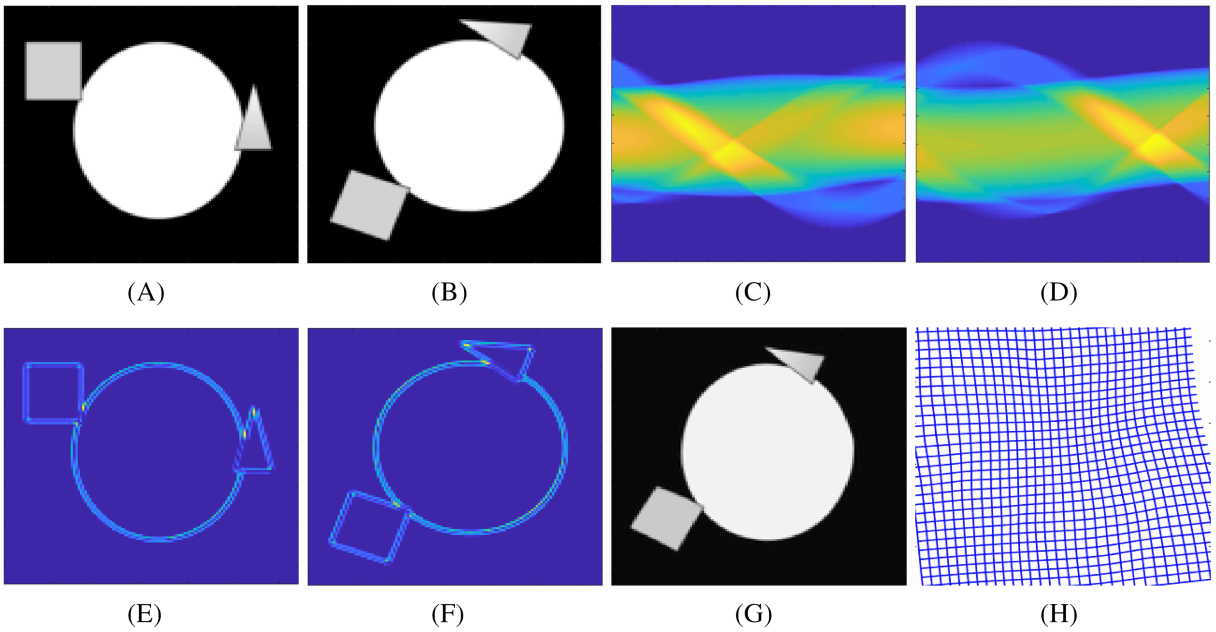

FIGURE 8 Example of a parametric monomodal image registration by using our model. The geometric transformation between the reference and the template images is in the form of a 70° rotation. (A) R: corresponding image for S_R. (B) T: corresponding image for S_T. (C) Reference sinogram S_R. (D) Template sinogram S_T. (E) RG: geometric information for S_R. (F) TG: geometric information for S_T. (G) Registered image $T(\varphi)$. (H) The deformation $\varphi(x) = x + \mathbf{u}(x)$ [Colour figure can be viewed at wileyonlinelibrary.com]

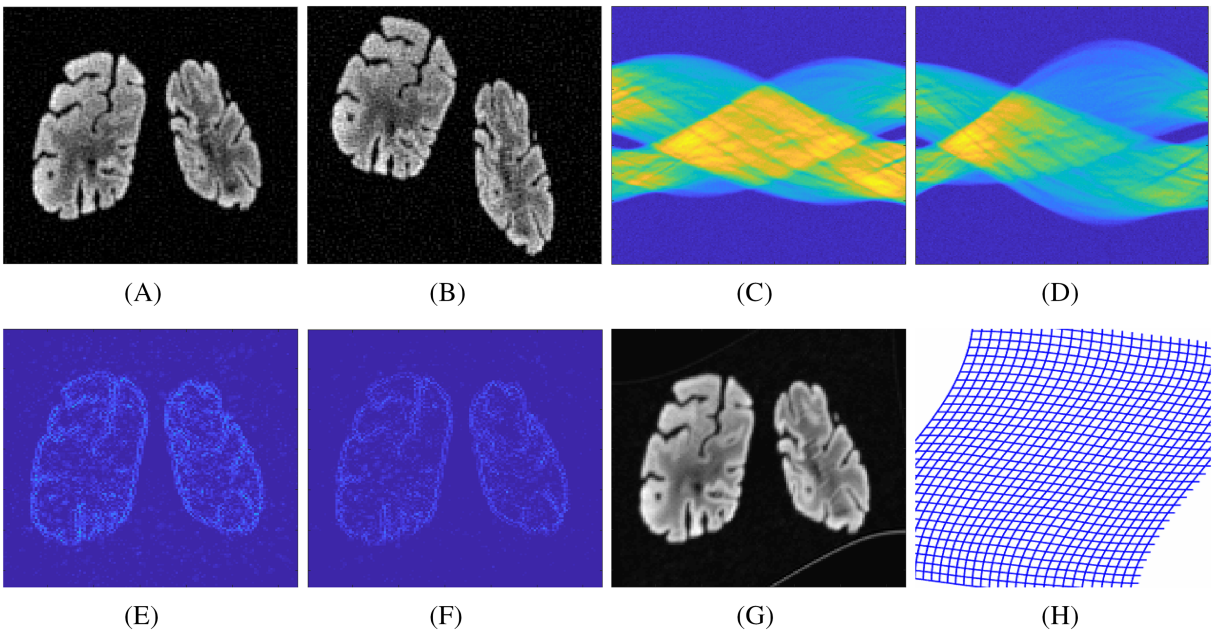

FIGURE 9 Example of a monomodal image registration by using our model in the case where we have noise in sinograms. We consider noisy sinograms S_R and S_T with an additive white Gaussian noise, with variance $N = 0.001$ and PSNR = 10.56. (A) R: corresponding image for S_R. (B) T: corresponding image for S_T. (C) Reference sinogram S_R. (D) Template sinogram S_T. (E) RG: geometric information for S_R. (F) TG: geometric information for S_T. (G) Registered image $T(\varphi)$, $\mathcal{E}_r = 0.22$. (H) The deformation $\varphi(x) = x + \mathbf{u}(x)$ [Colour figure can be viewed at wileyonlinelibrary.com]

Algorithm 3 Multilevel image registration: $U \leftarrow$ MLIR

Data: An initial guess U, minLevel and maxLevel from ML by computing a multilevel representation of both images.
Level = minLevel
while Level $\leq$ maxLevel **do**

1. $U_0 = U$
2. Solve the registration problem $U \leftarrow$ GNIR(U_0)
3. Level = next Level
4. Prolongate U to the finer grid: $U \longleftarrow$ prolongate(U)

end

6 | RESULTS AND DISCUSSION

In the sequel, we present some examples of the performance of our model, the sensitivity to the noise in the sinogram, and assess the quality of the registration results of the model by using the following error measure:

$$\mathcal{E}_r = \frac{\|RG - TG(\varphi)\|_2^2}{\|RG - TG\|_2^2}, \tag{25}$$

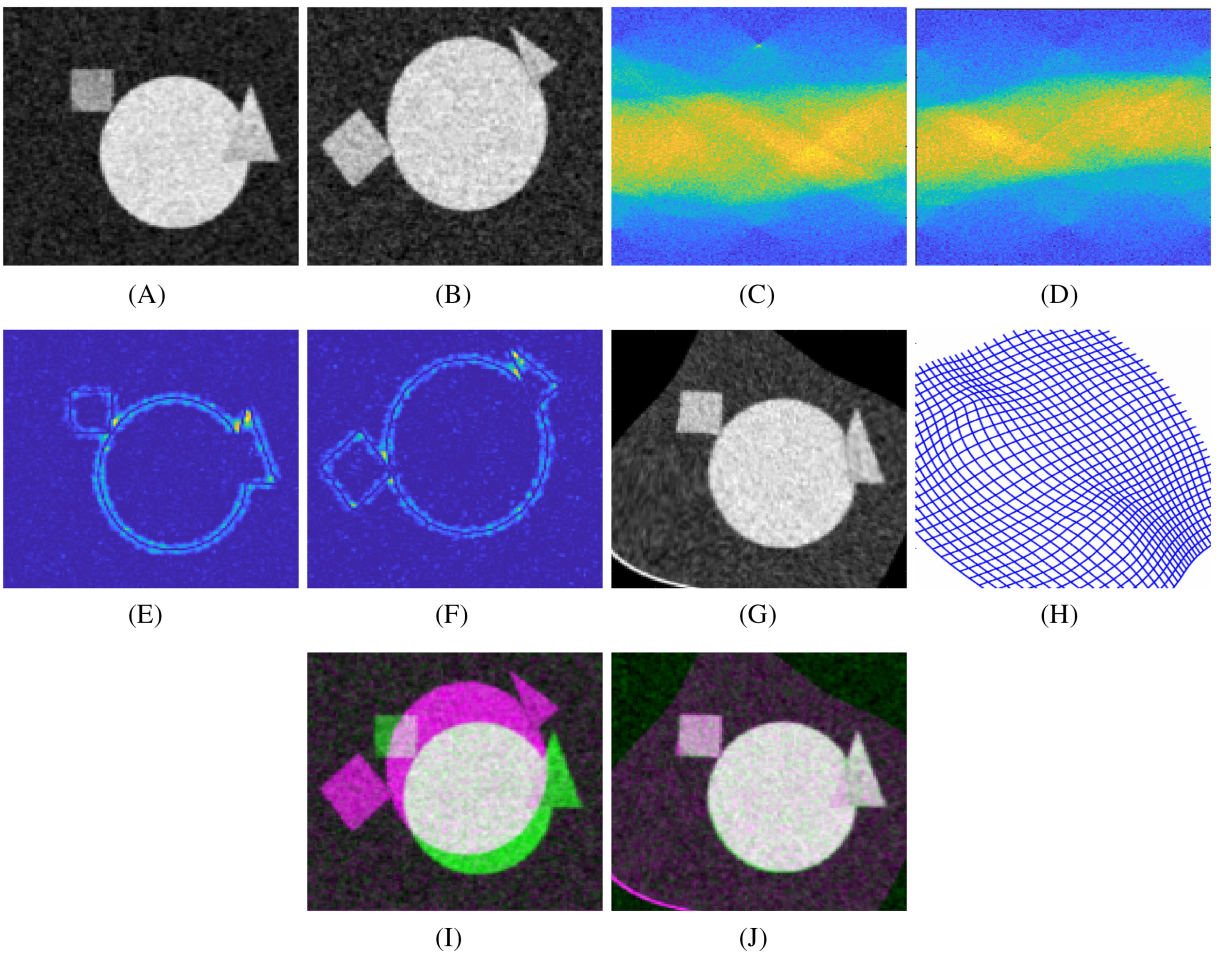

FIGURE 10 Example of monomodal images registration by using our model in the case where we have noise in sinograms. We consider noisy sinograms S_R and S_T with an additive white Gaussian noise, with variance $N = 0.6$. (A) R: corresponding image for S_R. (B) T: correspondence image for S_T. (C) Reference sinogram S_R. (D) Template sinogram S_T. (E) RG: geometric information for S_R. (F) TG: geometric information for S_T. (G) Registered image $T(\varphi)$, $\mathcal{E}_r = 0.11$. (H) The deformation $\varphi(x) = x + \mathbf{u}(x)$. (I) R and T before the registration. (J) R and T after the registration [Colour figure can be viewed at wileyonlinelibrary.com]

TABLE 2 Example of errors with different values of PSNR for Figure 10

Figure 10	PSNR	20.31	17.2	14.53	11.4
	$\mathcal{E}_r$	0.09	0.1	0.1	0.11

where $TG(\varphi)$ represents the registered geometric information. The run time for the image registration process is given in Table 1. In the presented examples, all the images are of size 128×128. The algorithms were implemented in MATLAB R2021b running on a laptop with Intel(R) core(TM) i5 processor, CPU at 2.50 GHz, and 8 GB RAM memory at 2133 MHz. Since our model is based on the Gauss–Newton method, a multilevel technique is used to accelerate the optimization process. The required run times show the speed of our model.

For each test, we present both images S_R and S_T which represent, respectively, the reference and the template sinogram, the correspondence images for S_R and S_T which are denoted respectively by R and T, the edges RG and TG which are used for defining our proposed image registration model, the registered image $T(\varphi)$, and the deformation $\varphi(\mathbf{u})(\mathbf{x}) = \mathbf{x} + \mathbf{u}(\mathbf{x})$.

In Figure 4, we have a multimodal images, the reference and the template images represent a cross section of the brain. Figure 5 is an example of a monomodal image registration with a nonparametric transformation. Clearly, we see that we have a perfect registered image with a relative error $\mathcal{E}_r = 0.08$.

In Figures 6–8, we display some examples of synthetic images for a monomodal images registration. In all cases, we have the same object in reference and template images but each template has different deformation. To evaluate our model, we took different rotation's degrees. Then, we can show that our model performs well for the degrees that are less than 70°. In Figures 9 and 10, to test the sensitivity of our model to the noise, we add white Gaussian noise, often abbreviated AWGN, in sinogram with variance $N = 0.001$ and $N = 0.6$, respectively. We show that our model performs well. Moreover, we tested our model with different noise level for Figure 10 and by checking the errors in Table 2, we could show that our proposed model performs well in the presence of noise.

7 | CONCLUSION

We have used the topological gradient approach for a tomographic reconstruction that uses the first- and second-order discontinuities. We have shown the advantage of that T-G which uses only the first-order discontinuities for the detection of geometric information. A new method for image registration with information geometric detection via the topological gradient method has been presented in this work. The results obtained for the detection and the registration are very promising.

ACKNOWLEDGEMENT

There are no funders to report for this submission.

CONFLICT OF INTEREST

This work does not have any conflicts of interest.

AUTHOR CONTRIBUTIONS

Mohamed Lajili conducted the formal analysis, conducted the investigation, validated the results, and wrote the original draft of the manuscript. Badreddine Rjaibi conducted the investigation, supervised the study, and reviewed and edited the manuscript. Didier Auroux conducted the investigation, supervised the study, and reviewed and edited the manuscript. Maher Moakher conducted the investigation, supervised the study, and reviewed and edited the manuscript.

ORCID

Mohamed Lajili https://orcid.org/0000-0002-9508-3587
Badreddine Rjaibi https://orcid.org/0000-0002-8482-6955
Didier Auroux https://orcid.org/0000-0002-8837-2807
Maher Moakher https://orcid.org/0000-0002-9432-0456

REFERENCES

1. Schindelin J, Rueden CT, Hiner MC, Eliceiri KW. The ImageJ ecosystem: an open platform for biomedical image analysis. *Molecul Reproduct Develop*. 2015;82(7–8):518-529.
2. Beroiz M, Cabral JB, Sanchez B. Astroalign: a Python module for astronomical image registration. *Astron Comput*. 2020;32:100384.
3. Quang TT, Chen WF, Papay FA, Liu Y. Dynamic, real-time, fiducial-free surgical navigation with integrated multimodal optical imaging. *IEEE Photonics J*. 2020;13(1):1-13.
4. Alavi A, Bar-Joseph Z. Iterative point set registration for aligning scRNA-seq data. *PLoS Comput Biol*. 2020;16(10):e1007939.
5. Zhang J, Hu J, Jiang Z, et al. Automatic 3D image registration for nano-resolution chemical mapping using synchrotron spectro-tomography. *J Synchrotron Radiation*. 2021;28(1):278-282.
6. Goshtasby AA. *2-D and 3-D Image Registration: For Medical, Remote Sensing, and Industrial Applications*: John Wiley & Sons; 2005.
7. Gigengack F, Ruthotto L, Burger M, Wolters CH, Jiang X, Schafers KP. Motion correction in dual gated cardiac PET using mass-preserving image registration. *IEEE Trans Med Imag*. 2011;31(3):698-712.
8. Modersitzki J. *FAIR: Flexible Algorithms for Image Registration*: SIAM; 2009.
9. Sotiras A, Davatzikos C, Paragios N. Deformable medical image registration: a survey. *IEEE Trans Med Imag*. 2013;32(7):1153-1190.
10. Theljani A, Chen K. An augmented Lagrangian method for solving a new variational model based on gradients similarity measures and high order regularization for multimodality registration. *Inverse Problems and Imaging*. 2019;13(2):309-335.
11. Hodneland E, Lundervold A, Rørvik J, Munthe-Kaas AZ. Normalized gradient fields for nonlinear motion correction of DCE-MRI time series. *Computerized Med Imag Graphics*. 2014;38(3):202-210.
12. König L, Rühaak J. A fast and accurate parallel algorithm for non-linear image registration using normalized gradient fields. In: 2014 IEEE 11th International Symposium on Biomedical Imaging (ISBI), Vol. 38. IEEE; 2014:580-583.
13. Ruhaak J, Konig L, Hallmann M, et al. A fully parallel algorithm for multimodal image registration using normalized gradient fields. In: IEEE 10th International Symposium on Biomedical Imaging, Vol. 38. IEEE; 2013:572-575.
14. Maes F, Collignon A, Vandermeulen D, Marchal G, Suetens P. Multimodality image registration by maximization of mutual information. *IEEE Trans Med Imaging*. 1997;16(2):187-198.
15. Pluim JPW, Maintz JBA, Viergever MA. Mutual-information-based registration of medical images: a survey. *IEEE Trans Med Imaging*. 2003;22(8):986-1004.
16. Hu W, Xie Y, Li L, Zhang W. A total variation based nonrigid image registration by combining parametric and non-parametric transformation models. *Neurocomputing*. 2014;144:222-237.
17. Fischer B, Modersitzki J. Fast diffusion registration. *Contemp Math*. 2002;313:117-128.
18. Zhang X-Q, Froment J. Total variation based Fourier reconstruction and regularization for computer tomography. In: IEEE Nuclear Science Symposium Conference Record, 2005, Vol. 4. IEEE; 2005:2332-2336.
19. Rudin LI, Osher S, Fatemi E. Nonlinear total variation based noise removal algorithms. *Phys D: Nonlin Phenom*. 1992;60(1-4):259-268.
20. Natterer F. *The mathematics of computerized tomography*, Classics in Applied Mathematics: SIAM; 2001.
21. Lewitt RM. Reconstruction algorithms: transform methods. *Proc IEEE*. 1983;71(3):390-408.
22. Houichet H, Theljani A, Rjaibi B, Moakher M. A nonstandard higher-order variational model for speckle noise removal and thin-structure detection. *J Math Study*. 2019;52:394-424.
23. Basu S, Bresler Y. $O(N^2\log_2 N)$ filtered backprojection reconstruction algorithm for tomography. *IEEE Trans Image Process*. 2000;9(10):1760-1773.
24. Deans SR. *The Radon Transform and Some of Its Applications*: Courier Corporation; 2007.
25. Blomgren P, Chan TF, Mulet P, Wong C-K. Total variation image restoration: numerical methods and extensions. In: Proceedings of International Conference on Image Processing, Vol. 3. IEEE; 1997:384-387.
26. Chan T, Marquina A, Mulet P. High-order total variation-based image restoration. *SIAM J Scientif Comput*. 2000;22(2):503-516.
27. Auroux D, Jaafar-Belaid L, Rjaibi B. Application of the topological gradient method to tomography. *Revue Africaine de la Recherche en Informatique et Mathématiques Appliquées*. 2010;13:91-104.
28. Auroux D, Masmoudi M. Image processing by topological asymptotic expansion. *J Math Imag Vision*. 2009;33(2):122-134.
29. Amstutz S, Novotny AA, Van Goethem N. Topological sensitivity analysis for elliptic differential operators of order 2m. *J Differ Equ*. 2014;256(4):1735-1770.
30. Aubert G, Drogoul A. Topological gradient for a fourth order operator used in image analysis. *ESAIM: Control, Optim Calc Var*. 2015;21(4):1120-1149.
31. Drogoul A. Numerical analysis of the topological gradient method for fourth order models and applications to the detection of fine structures in imaging. *SIAM J Imag Sci*. 2014;7(4):2700-2731.
32. Amstutz S, Fehrenbach J. Edge detection using topological gradients: a scale-space approach. *J Math Imag Vision*. 2015;52(2):249-266.
33. Amstutz S, Horchani I, Masmoudi M. Crack detection by the topological gradient method. *Control Cybern*. 2005;34:81-101.
34. Auroux D. From restoration by topological gradient to medical image segmentation via an asymptotic expansion. *Math Comput Modell*. 2009;49(11-12):2191-2205.
35. Belaid LJ, Jaoua M, Masmoudi M, Siala L. Image restoration and edge detection by topological asymptotic expansion. *Comptes Rendus Math*. 2006;342(5):313-318.
36. Lajili M, Rjaibi B, Theljani A, Maher M. Edge sketches for multi-modal image registration based on Blake-Zisserman type energy. *Comput Appl Math*. 2022;41(7):1-20.

37. Zhang D, Theljani A, Chen K. On a new diffeomorphic multi-modality image registration model and its convergent Gauss-Newton solver. *J Math Res Appl*. 2019;39(6):633-656.

How to cite this article: Lajili M, Rjaibi B, Auroux D, Moakher M. Edge detection from X-ray tomographic data for geometric image registration. *Math Meth Appl Sci*. 2022;1-35. doi:10.1002/mma.8905

APPENDIX A: PROOF OF THEOREM 1

In this section, we establish the proof of the expressions of the three real numbers δ_a, δ_l, and δ_J. In this section, $x_0 = 0$ is taken for simplicity reasons.

As $l_\varepsilon(\cdot)$ is an independent linear form of ε, then we have $\delta_l = 0$.

A.1 | Estimate of δ_a

We have

$$\begin{aligned}(a_\varepsilon - a_0)(u_0, v_\varepsilon) &= \int_\Omega (\alpha_\varepsilon - \alpha_0)\Delta u_0 \Delta v_\varepsilon dx + \int_\Omega (\beta_\varepsilon - \beta_0)\nabla u_0 \nabla v_\varepsilon dx,\\ &= \int_{\omega_\varepsilon} (\alpha_1 - \alpha_0)\Delta u_0 \Delta v_\varepsilon dx + \int_{\omega_\varepsilon} (\beta_1 - \beta_0)\nabla u_0 \nabla v_\varepsilon dx,\\ &= \int_{\omega_\varepsilon} (\alpha_1 - \alpha_0)\Delta u_0 \Delta (v_\varepsilon - v_0) dx + \int_{\omega_\varepsilon} (\alpha_1 - \alpha_0)\Delta u_0 \Delta v_0 dx\\ &\quad + \int_{\omega_\varepsilon} (\beta_1 - \beta_0)\nabla u_0 \nabla (v_\varepsilon - v_0) dx + \int_{\omega_\varepsilon} (\beta_1 - \beta_0)\nabla u_0 \nabla v_0 dx.\end{aligned}$$

We notice $w_\varepsilon = v_\varepsilon - v_0$, then we obtain

$$\begin{aligned}(a_\varepsilon - a_0)(u_0, v_\varepsilon) &= \int_{\omega_\varepsilon} (\alpha_1 - \alpha_0)\Delta u_0 \Delta w_\varepsilon dx + \int_{\omega_\varepsilon} (\alpha_1 - \alpha_0)\Delta u_0 \Delta v_0 dx\\ &\quad + \int_{\omega_\varepsilon} (\beta_1 - \beta_0)\nabla u_0 \nabla w_\varepsilon dx + \int_{\omega_\varepsilon} (\beta_1 - \beta_0)\nabla u_0 \nabla v_0 dx.\end{aligned}$$

We have v_0 and v_ε solution of the following problems, respectively:

$$\begin{cases}\Delta(\alpha_0 \Delta v_0) - \operatorname{div}(\beta_0 \nabla v_0) + R^* R v_0 + \mu v_0 = -DJ_0(u_0), & \text{in } \Omega,\\ \frac{\partial(\alpha_0 \Delta v_0)}{\partial n} - \beta_0 \frac{\partial v_0}{\partial n} = 0, & \text{on } \partial\Omega,\\ \Delta v_0 = 0, & \text{on } \partial\Omega,\end{cases} \tag{A1}$$

and

$$\begin{cases}\Delta(\alpha_\varepsilon \Delta v_\varepsilon) - \operatorname{div}(\beta_\varepsilon \nabla v_\varepsilon) + R^* R v_\varepsilon + \mu v_\varepsilon = -DJ_\varepsilon(u_0), & \text{in } \Omega,\\ \frac{\partial \Delta(\alpha_\varepsilon v_\varepsilon)}{\partial n} - \beta_\varepsilon \frac{\partial v_\varepsilon}{\partial n} = 0, & \text{on } \partial\Omega,\\ \Delta v_\varepsilon = 0, & \text{on } \partial\Omega,\end{cases} \tag{A2}$$

Then, we deduce that $w_\varepsilon = v_\varepsilon - v_0$ is a solution of the following problem:

$$\begin{cases} \Delta(\alpha_\varepsilon \Delta w_\varepsilon) - \operatorname{div}(\beta_\varepsilon \nabla w_\varepsilon) + R^* R w_\varepsilon + \mu w_\varepsilon = G_\varepsilon, & \text{in } \Omega, \\ \frac{\partial(\alpha_\varepsilon \Delta w_\varepsilon)}{\partial n} - \beta_\varepsilon \frac{\partial w_\varepsilon}{\partial n} = g_\varepsilon, & \text{on } \partial\Omega, \\ \Delta w_\varepsilon = 0, & \text{on } \partial\Omega, \end{cases} \tag{A3}$$

where

$$\begin{aligned} G_\varepsilon &= \Delta((\alpha_0 - \alpha_\varepsilon)\Delta v_0) + \operatorname{div}((\beta_\varepsilon - \beta_0)\nabla v_0) + 2\Delta((\alpha_0 - \alpha_\varepsilon)\Delta u_0) + 2\operatorname{div}((\beta_\varepsilon - \beta_0)\nabla u_0), \\ g_\varepsilon &= \frac{\partial((\alpha_0 - \alpha_\varepsilon)\Delta v_0)}{\partial n} + (\beta_\varepsilon - \beta_0)\frac{\partial v_0}{\partial n}. \end{aligned}$$

By multiplying the first equation of (A3) with a function $w_\varepsilon \in \mathcal{V}$, and integrating over Ω, we obtain

$$\int_\Omega \Delta(\alpha_\varepsilon \Delta w_\varepsilon) w_\varepsilon dx - \int_\Omega \operatorname{div}(\beta_\varepsilon \nabla w_\varepsilon) w_\varepsilon dx + \int_\Omega (R^* R w_\varepsilon) \cdot w_\varepsilon dx + \mu \int_\Omega |w_\varepsilon|^2 dx = \int_\Omega G_\varepsilon w_\varepsilon dx.$$

By applying Green's formula, we obtain

$$\begin{aligned} \int_\Omega G_\varepsilon w_\varepsilon dx = &- \int_\Omega \nabla(\alpha_\varepsilon \Delta w_\varepsilon) \nabla w_\varepsilon dx + \int_{\partial\Omega} \frac{\partial(\alpha_\varepsilon \Delta w_\varepsilon)}{\partial n} w_\varepsilon d\sigma + \int_\Omega \beta_\varepsilon |\nabla w_\varepsilon|^2 dx \\ &- \int_{\partial\Omega} \beta_\varepsilon \frac{\partial w_\varepsilon}{\partial n} w_\varepsilon d\sigma + \int_\Omega (R^* R w_\varepsilon) \cdot w_\varepsilon dx + \mu \int_\Omega |w_\varepsilon|^2 dx. \end{aligned}$$

Moreover,

$$\frac{\partial \Delta(\alpha_\varepsilon w_\varepsilon)}{\partial n} - \beta_\varepsilon \frac{\partial w_\varepsilon}{\partial n} = g_\varepsilon \text{ on } \partial\Omega,$$

which gives

$$\begin{aligned} \int_\Omega G_\varepsilon w_\varepsilon dx = &\int_\Omega \alpha_\varepsilon |\Delta w_\varepsilon|^2 dx - \int_{\partial\Omega} \alpha_\varepsilon \Delta w_\varepsilon \nabla w_\varepsilon \vec{n} d\sigma + \int_{\partial\Omega} g_\varepsilon w_\varepsilon d\sigma \\ &+ \int_\Omega \beta_\varepsilon |\nabla w_\varepsilon|^2 dx + \int_\Omega (R^* R w_\varepsilon) \cdot w_\varepsilon dx + \mu \int_\Omega |w_\varepsilon|^2 dx. \end{aligned}$$

Using the fact that $\Delta w_\varepsilon = 0$ on $\partial\Omega$, we deduce

$$\begin{aligned} \int_\Omega G_\varepsilon w_\varepsilon dx - \int_{\partial\Omega} g_\varepsilon w_\varepsilon d\sigma &= \int_\Omega \alpha_\varepsilon |\Delta w_\varepsilon|^2 dx + \int_\Omega \beta_\varepsilon |\nabla w_\varepsilon|^2 dx + \int_\Omega (R^* R w_\varepsilon) \cdot w_\varepsilon dx + \mu \int_\Omega |w_\varepsilon|^2 dx. \\ &\geq \min(\alpha_\varepsilon) \|\Delta w_\varepsilon\|^2_{L^2(\Omega)} + \min(\beta_\varepsilon) \|\nabla w_\varepsilon\|^2_{L^2(\Omega)} + \|R w_\varepsilon\|^2_{L^2(\Omega)} + \mu \|w_\varepsilon\|^2_{L^2(\Omega)}, \end{aligned}$$

which implies that

$$\int_\Omega G_\varepsilon w_\varepsilon dx - \int_{\partial\Omega} g_\varepsilon w_\varepsilon d\sigma \geq \min(\alpha_\varepsilon) \|\Delta w_\varepsilon\|^2_{L^2(\Omega)} + \min(\beta_\varepsilon) \|\nabla w_\varepsilon\|^2_{L^2(\Omega)} + \mu \|w_\varepsilon\|^2_{L^2(\Omega)}.$$

Hence, there exists $c = \min(\alpha_0, \alpha_1, \beta_0, \beta_1, \mu)$ such that

$$c \|w_\varepsilon\|^2_{H^2(\Omega)} \leq \int_\Omega G_\varepsilon w_\varepsilon dx - \int_{\partial\Omega} g_\varepsilon w_\varepsilon d\sigma.$$

On the other hand, we have

$$\begin{aligned}\int_\Omega G_\varepsilon w_\varepsilon dx - \int_{\partial\Omega} g_\varepsilon w_\varepsilon d\sigma = &\int_\Omega \Delta((\alpha_0-\alpha_\varepsilon)\Delta v_0)w_\varepsilon + \ \operatorname{div}((\beta_\varepsilon-\beta_0)\nabla v_0)w_\varepsilon dx\\ &+2\int_\Omega \Delta((\alpha_0-\alpha_\varepsilon)\Delta u_0)w_\varepsilon + \operatorname{div}((\beta_\varepsilon-\beta_0)\nabla u_0)w_\varepsilon dx\\ &+\int_{\partial\Omega}\frac{\partial((\alpha_\varepsilon-\alpha_0)\Delta v_0)}{\partial n}w_\varepsilon d\sigma + \int_{\partial\Omega}(\beta_0-\beta_\varepsilon)\frac{\partial v_0}{\partial n}w_\varepsilon d\sigma.\end{aligned}$$

Then, by applying Hölder's inequality, we deduce

$$\begin{aligned}c\|w_\varepsilon\|^2_{H^2(\Omega)} \le &\left[\int_\Omega [\Delta((\alpha_0-\alpha_\varepsilon)\Delta v_0)]^2 dx\right]^{\frac12}\|w_\varepsilon\|_{L^2(\Omega)} + \left[\int_\Omega [\operatorname{div}((\beta_\varepsilon-\beta_0)\nabla v_0)]^2 dx\right]^{\frac12}\|w_\varepsilon\|_{L^2(\Omega)}\\ &+2\left[\int_\Omega [\Delta(\alpha_0-\alpha_\varepsilon)(\Delta u_0)]^2 dx\right]^{\frac12}\|w_\varepsilon\|_{L^2(\Omega)} + 2\left[\int_\Omega [\operatorname{div}((\beta_\varepsilon-\beta_0)\nabla u_0)]^2 dx\right]^{\frac12}\|w_\varepsilon\|_{L^2(\Omega)}\\ &+\left[\int_{\partial\Omega}\left(\frac{\partial((\alpha_\varepsilon-\alpha_0)\Delta v_0)}{\partial n}\right)^2 d\sigma\right]^{\frac12}\|w_\varepsilon\|_{0,\partial\Omega} + \left[\int_{\partial\Omega}(\beta_0-\beta_\varepsilon)^2\left(\frac{\partial v_0}{\partial n}\right)^2 d\sigma\right]^{\frac12}\|w_\varepsilon\|_{0,\partial\Omega}.\end{aligned}$$

By using the trace theorem and the fact that embeddings $H^2(\Omega)\hookrightarrow H^1(\Omega)\hookrightarrow L^2(\Omega)$ are continuous, we have

$$\begin{cases}\|w_\varepsilon\|_{0,\partial\Omega}\le c\|w_\varepsilon\|_{1,\Omega},\\ \|w_\varepsilon\|_{0,\Omega}\le\|w_\varepsilon\|_{2,\Omega},\\ \|w_\varepsilon\|_{1,\Omega}\le\|w_\varepsilon\|_{2,\Omega}.\end{cases}$$

So we deduce that

$$\|w_\varepsilon\|_{2,\Omega}\le C_1[A+B+C+D+E+F], \tag{A4}$$

where

$$\begin{aligned}A^2 &= \int_\Omega [\Delta((\alpha_0-\alpha_\varepsilon)\Delta v_0)]^2 dx,\\ B^2 &= \int_\Omega (\operatorname{div}((\beta_\varepsilon-\beta_0)\nabla v_0))^2 dx,\\ C^2 &= \int_\Omega [\Delta((\alpha_0-\alpha_\varepsilon)\Delta u_0)]^2 dx,\\ D^2 &= \int_\Omega [\operatorname{div}((\beta_\varepsilon-\beta_0)\nabla u_0)]^2 dx,\\ E^2 &= \int_{\partial\Omega}\left(\frac{\partial(\alpha_\varepsilon-\alpha_0)\Delta v_0}{\partial n}\right)^2 d\sigma,\\ F^2 &= \int_{\partial\Omega}(\beta_0-\beta_\varepsilon)^2\left(\frac{\partial v_0}{\partial n}\right)^2 d\sigma.\end{aligned}$$

Lemma A.1. *We have*

$$E^2 = F^2 = 0.$$

Proof. We have $\alpha_\varepsilon = \alpha_0$ (respectively, $\beta_\varepsilon = \beta_0$) on $\Omega\backslash\overline{\omega_\varepsilon}$, then according to the trace theorem, we deduce $\alpha_\varepsilon = \alpha_0$ (respectively, $\beta_\varepsilon = \beta_0$) on $\partial\Omega_\varepsilon = \partial\Omega \cup \partial\omega_\varepsilon$. Then, $E^2 = F^2 = 0$. □

Lemma A.2. *We have*

$$A = \left[\int_\Omega [\Delta((\alpha_0 - \alpha_\varepsilon)\Delta v_0)]^2 dx\right]^{\frac{1}{2}} = O(\varepsilon).$$

Proof. We have

$$\begin{aligned} A^2 &= \int_\Omega [\Delta((\alpha_0 - \alpha_\varepsilon)\Delta v_0)]^2 dx, \\ &= \int_{\omega_\varepsilon} [\Delta((\alpha_0 - \alpha_1)\Delta v_0)]^2 dx, \\ &= (\alpha_0 - \alpha_1)^2 \int_{\omega_\varepsilon} (\Delta^2 v_0(x))^2 - (\Delta^2 v_0(0))^2 + (\Delta^2 v_0(0))^2 dx. \end{aligned}$$

Using the following change of variable $\left(\frac{x_1}{a}, \frac{x_2}{b}\right) = \varepsilon z$, we obtain

$$A^2 = (\alpha_0 - \alpha_1)^2 \int_{B(0,1)} [(\Delta^2 v_0(\varepsilon z))^2 - (\Delta^2 v_0(0))^2]\varepsilon^2 ab dz + (\alpha_0 - \alpha_1)^2 (\Delta^2 v_0(0))^2 \varepsilon^2 ab\pi.$$

As $\Delta^2 v_0$ is continuous in a neighborhood of 0, then there exists $M > 0$ such that

$$|\Delta^2 v_0(\varepsilon z)^2 - \Delta^2 v_0(0)^2| \leq M.$$

Thus,

$$A^2 \leq (\alpha_0 - \alpha_1)^2 \varepsilon^2 ab\pi (M + (\Delta^2 v_0(0))^2),$$

and therefore,

$$A^2 = O(\varepsilon^2) \Rightarrow A = O(\varepsilon).$$

□

Lemma A.3. *We have*

$$B = \left[\int_\Omega (div((\beta_\varepsilon - \beta_0)\nabla v_0))^2 dx\right]^{\frac{1}{2}} = O(\varepsilon),$$

$$C = \left[\int_\Omega [\Delta((\alpha_0 - \alpha_\varepsilon)\Delta u_0)]^2 dx\right]^{\frac{1}{2}} = O(\varepsilon),$$

$$D = \left[\int_\Omega (div((\beta_\varepsilon - \beta_0)\nabla u_0))^2 dx\right]^{\frac{1}{2}} = O(\varepsilon).$$

Proof. We have

$$B^2 = \int_{\Omega} (\mathrm{div}((\beta_\varepsilon - \beta_0)\nabla v_0))^2 dx = \int_{\omega_\varepsilon} (\beta_1 - \beta_0)^2 (\Delta v_0)^2 dx,$$
$$= (\beta_1 - \beta_0)^2 \left[\int_{\omega_\varepsilon} (\Delta v_0(x))^2 - (\Delta v_0(0))^2 dx + \int_{\omega_\varepsilon} (\Delta v_0(0))^2 dx \right].$$

Using the following change of variable $\left(\frac{x_1}{a}, \frac{x_2}{b}\right) = \varepsilon z$, we obtain

$$B^2 = (\beta_1 - \beta_0)^2 \left[\varepsilon^2 ab \int_{B(0,1)} (\Delta v_0(\varepsilon z))^2 - (\Delta v_0(0))^2 dz + \varepsilon^2 ab\pi \Delta v_0(0))^2 \right].$$

As Δv_0 is continuous in a neighborhood of 0, we obtain:

$$|(\Delta v_0(\varepsilon z))^2 - (\Delta v_0(0))^2| = o(1).$$

Then, there exists $M > 0$ such that

$$B^2 \leq (\beta_1 - \beta_0)^2 \varepsilon^2 ab\pi \left[M + (\Delta v_0(0))^2 \right],$$

which implies that

$$B^2 = O(\varepsilon^2) \Rightarrow B = O(\varepsilon).$$

By using some classical computation techniques, we obtain

$$C^2 = O(\varepsilon^2) \Rightarrow C = O(\varepsilon),$$
$$D^2 = O(\varepsilon^2) \Rightarrow D = O(\varepsilon).$$

□

According to inequality (A4) and Lemmas A.1–A.3, we deduce that

$$\|w_\varepsilon\|_{H^2(\Omega)} = O(\varepsilon). \tag{A5}$$

Lemma A.4. *We have*

$$\int_{\omega_\varepsilon} \nabla u_0 \nabla w_\varepsilon dx = o(\varepsilon^2).$$

Proof. We have

$$\left| \int_{\omega_\varepsilon} \nabla u_0 \nabla w_\varepsilon dx \right| \leq \|\nabla u_0\|_{L^\infty(\omega\varepsilon)} \int_{\omega_\varepsilon} |\nabla w_\varepsilon| dx.$$

By applying Hölder's inequality for $p, q \in [1, +\infty]$ such that $\frac{1}{p} + \frac{1}{q} = 1$, we obtain

$$\left| \int_{\omega_\varepsilon} \nabla u_0 \nabla w_\varepsilon dx \right| \leq c \left(\int_{\omega_\varepsilon} 1 dx \right)^{\frac{1}{p}} \|\nabla w_\varepsilon\|_{L^q(\omega_\varepsilon)} \leq c\left(\varepsilon^2 ab\right)^{\frac{1}{p}} \|\nabla w_\varepsilon\|_{L^q(\omega_\varepsilon)}.$$

Choosing $p = \frac{3}{2}$ and $q = 3$ in the above and since the embedding $L^3(\Omega) \hookrightarrow L^2(\Omega)$ is continuous, we obtain

$$\left| \int_{\omega_\varepsilon} \nabla u_0 \nabla w_\varepsilon dx \right| \leq c\left(\varepsilon^2 ab\right)^{\frac{2}{3}} \|\nabla w_\varepsilon\|_{L^2(\Omega)} \leq c\left(\varepsilon^2 ab\right)^{\frac{2}{3}} \|w_\varepsilon\|_{H^2(\Omega)}.$$

Moreover

$$\|w_\varepsilon\|_{H^2(\Omega)} = O(\varepsilon).$$

Then,

$$\left| \int_{\omega_\varepsilon} \nabla u_0 \nabla w_\varepsilon dx \right| \leq c\varepsilon^{\frac{7}{3}} (ab)^{\frac{2}{3}},$$

which implies

$$\int_{\omega_\varepsilon} \nabla u_0 \nabla w_\varepsilon dx = o(\varepsilon^2).$$

□

Lemma A.5. *We have*

$$\int_{\omega_\varepsilon} \Delta u_0 \Delta w_\varepsilon dx = -\varepsilon^2 (k_0^{a,b} + 1)\Delta v_0(x_0) \left(k_1^{a,b} \frac{\partial^2 u_0(x_0)}{\partial x^2} + k_2^{a,b} \frac{\partial^2 u_0(x_0)}{\partial y^2} + k_3^{a,b} \left(\frac{\partial^2 u_0(x_0)}{\partial x \partial y} + \frac{\partial^2 u_0(x_0)}{\partial y \partial x} \right) \right) + o(\varepsilon^2),$$

where

$$k_0^{a,b} = \frac{2\pi}{\frac{1}{2}\int_0^{2\pi} \sqrt{a^2\cos^2(\theta) + b^2\sin^2(\theta)} d\theta - \pi},$$

$$k_1^{a,b} = \int_0^{2\pi} \frac{a^2\cos^2(\theta)}{\sqrt{a^2\cos^2(\theta) + b^2\sin^2(\theta)}} d\theta,$$

$$k_2^{a,b} = \int_0^{2\pi} \frac{b^2\sin^2(\theta)}{\sqrt{a^2\cos^2(\theta) + b^2\sin^2(\theta)}} d\theta,$$

$$k_3^{a,b} = \int_0^{2\pi} \frac{ab\cos(\theta)\sin(\theta)}{\sqrt{a^2\cos^2(\theta) + b^2\sin^2(\theta)}} d\theta.$$

Proof. By applying Green's formula, we obtain

$$\int_{\omega_\varepsilon} \Delta u_0 \Delta w_\varepsilon dx = -\int_{\omega_\varepsilon} \nabla(\Delta u_0) \nabla w_\varepsilon dx + \int_{\partial\omega_\varepsilon} \frac{\partial \omega_\varepsilon}{\partial n} \Delta u_0 dx,$$

$$= \int_{\omega_\varepsilon} \Delta^2 u_0 w_\varepsilon dx - \int_{\partial\omega_\varepsilon} w_\varepsilon \frac{\partial \Delta u_0}{\partial n} d\sigma + \int_{\partial\omega_\varepsilon} \frac{\partial w_\varepsilon}{\partial n} \Delta u_0 dx.$$

As $\Delta^2 u_0$ is continuous in a neighborhood of x_0, we get

$$\left| \int_{\omega_\varepsilon} \Delta^2 u_0 w_\varepsilon dx \right| \leq \|\Delta^2 u_0\|_{L^\infty(\omega_\varepsilon)} \int_{\omega_\varepsilon} |w_\varepsilon| dx \leq c(ab)^{\frac{3}{4}} \varepsilon^{\frac{5}{2}}.$$

Then,

$$\int_{\omega_\varepsilon} \Delta^2 u_0 w_\varepsilon dx = o(\varepsilon^2),$$

and according to Appendix B, we have

$$\int_{\partial\omega_\varepsilon} \frac{\partial \Delta u_0}{\partial n} w_\varepsilon d\sigma = o(\varepsilon^2),$$

and

$$\int_{\partial\omega_\varepsilon} \Delta u_0 \frac{\partial w_\varepsilon}{\partial n} d\sigma = -\varepsilon^2 (k_0^{a,b} + 1) \Delta v_0(x_0) \left(k_1^{a,b} \frac{\partial^2 u_0(x_0)}{\partial x^2} + k_2^{a,b} \frac{\partial^2 u_0(x_0)}{\partial y^2} + k_3^{a,b} \left(\frac{\partial^2 u_0(x_0)}{\partial x \partial y} + \frac{\partial^2 u_0(x_0)}{\partial y \partial x} \right) \right) + o(\varepsilon^2).$$

Then, we obtain

$$\begin{aligned} \int_{\omega_\varepsilon} \Delta u_0 \Delta w_\varepsilon dx = &- \varepsilon^2 (k_0^{a,b} + 1) \Delta v_0(x_0) \left(k_1^{a,b} \frac{\partial^2 u_0(x_0)}{\partial x^2} + k_2^{a,b} \frac{\partial^2 u_0(x_0)}{\partial y^2} \right. \\ &\left. + k_3^{a,b} \left(\frac{\partial^2 u_0(x_0)}{\partial x \partial y} + \frac{\partial^2 u_0(x_0)}{\partial y \partial x} \right) \right) + o(\varepsilon^2). \end{aligned}$$

□

Lemma A.6. *We have*

$$\int_{\omega_\varepsilon} \nabla u_0 \nabla v_0 dx = \varepsilon^2 ab\pi \nabla u_0(0) \nabla v_0(0) + o(\varepsilon^2).$$

Proof. We have

$$\int_{\omega_\varepsilon} \nabla u_0 \nabla v_0(x) dx = \int_{\omega_\varepsilon} (\nabla u_0 \nabla v_0)(x) - (\nabla u_0 \nabla v_0)(0) dx + \int_{\omega_\varepsilon} (\nabla u_0 \nabla v_0)(0) dx.$$

By using the following change of variable $\left(\frac{x_1}{a}, \frac{x_2}{b}\right) = \varepsilon z$, we obtain

$$\int_{\omega_\varepsilon} (\nabla u_0 \nabla v_0)(x) dx = \int_{B(0,1)} ab\varepsilon^2 \left[(\nabla u_0 \nabla v_0)(\varepsilon z) - (\nabla u_0 \nabla v_0)(0) \right] dz + \varepsilon^2 ab\pi (\nabla u_0 \nabla v_0)(0).$$

By applying the first-order Taylor formula in the neighborhood of 0, we obtain

$$|\nabla u_0(\varepsilon z) \nabla v_0(\varepsilon z) - \nabla u_0(0) \nabla v_0(0)| = O(\varepsilon).$$

Thus,

$$\int_{\omega_\varepsilon} (\nabla u_0 \nabla v_0)(x) dx = o(\varepsilon^2) + \varepsilon^2 ab\pi \nabla u_0(0) \nabla v_0(0).$$

□

Lemma A.7. *We have*

$$\int_{\omega_\varepsilon} (\Delta u_0 \Delta v_0)(x)dx = \varepsilon^2 ab\pi \Delta u_0(0)\Delta v_0(0) + o(\varepsilon^2).$$

Proof. We have

$$\int_{\omega_\varepsilon} (\Delta u_0 \Delta v_0)(x)dx = \int_{\omega_\varepsilon} (\Delta u_0 \Delta v_0)(x) - (\Delta u_0 \Delta v_0)(0)dx + \int_{\omega_\varepsilon} (\Delta u_0 \Delta v_0)(0)dx.$$

By applying the change of variable $\left(\frac{x_1}{a}, \frac{x_2}{b}\right) = \varepsilon z$, we obtain

$$\int_{\omega_\varepsilon} (\Delta u_0 \Delta v_0)(x)dx = \int_{B(0,1)} ab\varepsilon^2 \left[(\Delta u_0 \Delta v_0)(\varepsilon z) - (\Delta u_0 \Delta v_0)(0)\right] dz + \varepsilon^2 ab\pi (\Delta u_0 \Delta v_0)(0).$$

By applying the first-order Taylor formula in the neighborhood of 0, we obtain

$$|\Delta u_0(\varepsilon z)\Delta v_0(\varepsilon z) - \Delta u_0(0)\Delta v_0(0)| = O(\varepsilon).$$

Then,

$$\int_{\omega_\varepsilon} (\Delta u_0 \Delta v_0)(x)dx = \varepsilon^2 ab\pi \Delta u_0(0)\Delta v_0(0) + o(\varepsilon^2).$$

□

A.2 | Estimation of δ_J

The estimation of δ_J is based on the following hypothesis:

$$J_\varepsilon(u_\varepsilon) - J_0(u_0) = DJ_\varepsilon(u_0)(u_\varepsilon - u_0) + f(\varepsilon)\delta_J + o(f(\varepsilon)). \tag{A6}$$

We have

$$\begin{aligned} J_\varepsilon(u_\varepsilon) - J_0(u_0) &= \left[\int_\Omega \alpha_\varepsilon |\Delta u_\varepsilon|^2 dx - \int_\Omega \alpha_0 |\Delta u_0|^2 dx\right] + \left[\int_\Omega \beta_\varepsilon |\nabla u_\varepsilon|^2 dx - \int_\Omega \beta_0 |\nabla u_0|^2 dx\right], \\ &= K_\varepsilon^1 + K_\varepsilon^2. \end{aligned}$$

According to Lemmas A.8,A.9, and A.12, we get

$$K_\varepsilon^1 = (\alpha_1 - \alpha_0)ab\pi\varepsilon^2 |\Delta u_0(0)|^2 + 2\int_\Omega \alpha_\varepsilon \Delta u_0 \Delta(u_\varepsilon - u_0)dx + o(\varepsilon^2) + \int_\Omega \alpha_\varepsilon |\Delta(u_\varepsilon - u_0)|^2 dx,$$

$$K_\varepsilon^2 = (\beta_1 - \beta_0)ab\pi\varepsilon^2 |\nabla u_0(0)|^2 + 2\int_\Omega \beta_\varepsilon \nabla u_0 \nabla(u_\varepsilon - u_0)dx + o(\varepsilon^2) + \int_\Omega \beta_\varepsilon |\nabla(u_\varepsilon - u_0)|^2 dx.$$

$$\int_\Omega \beta_\varepsilon |\nabla(u_\varepsilon - u_0)|^2 dx + \int_\Omega \alpha_\varepsilon |\Delta(u_\varepsilon - u_0)|^2 dx = o(\varepsilon^2).$$

Then, we obtain

$$J_\varepsilon(u_\varepsilon) - J_0(u_0) = ab\pi\varepsilon^2 \left[(\alpha_1 - \alpha_0)|\Delta u_0(0)|^2 + (\beta_1 - \beta_0)|\nabla u_0(0)|^2\right] + DJ_\varepsilon(u_0)(u_\varepsilon - u_0) + o(\varepsilon^2).$$

Lemma A.8. *We have*

$$\int_\Omega \alpha_\varepsilon |\Delta u_\varepsilon|^2 dx - \int_\Omega \alpha_0 |\Delta u_0|^2 dx = (\alpha_1 - \alpha_0) ab\pi\varepsilon^2 |\Delta u_0(0)|^2 + \int_\Omega \alpha_\varepsilon |\Delta(u_\varepsilon - u_0)|^2 dx + 2\int_\Omega \alpha_\varepsilon \Delta u_0 \Delta(u_\varepsilon - u_0) dx + o(\varepsilon^2).$$

Proof. We have

$$\begin{aligned}\int_\Omega \alpha_\varepsilon |\Delta u_\varepsilon|^2 dx - \int_\Omega \alpha_0 |\Delta u_0|^2 dx &= \int_\Omega \alpha_\varepsilon |\Delta u_\varepsilon|^2 dx - \int_\Omega ((\alpha_0 - \alpha_\varepsilon) + \alpha_\varepsilon) |\Delta u_0|^2 dx, \\ &= -\int_\Omega (\alpha_0 - \alpha_\varepsilon) |\Delta u_0|^2 dx + \int_\Omega \alpha_\varepsilon (|\Delta u_\varepsilon|^2 - |\Delta u_0|^2) dx, \\ &= -\int_{\omega_\varepsilon} (\alpha_0 - \alpha_1) |\Delta u_0|^2 dx + \int_\Omega \alpha_\varepsilon \left(|\Delta u_\varepsilon|^2 - |\Delta u_0|^2\right) dx.\end{aligned}$$

On the one hand, we have

$$\int_{\omega_\varepsilon} |\Delta u_0(x)|^2 dx = \int_{\omega_\varepsilon} \left[|\Delta u_0(x)|^2 - |\Delta u_0(0)|^2\right] dx + \int_{\omega_\varepsilon} |\Delta u_0(0)|^2 dx.$$

By using the change of variable $\left(\frac{x_1}{a}, \frac{x_2}{b}\right) = \varepsilon z$ and applying the first-order Taylor formula in the neighborhood of zero, we get

$$\int_{\omega_\varepsilon} |\Delta u_0(x)|^2 dx = o(\varepsilon^2) + ab\pi\varepsilon^2 |\Delta u_0(0)|^2.$$

Furthermore, we have

$$\begin{aligned}\int_\Omega \alpha_\varepsilon \left(|\Delta u_\varepsilon|^2 - |\Delta u_0|^2\right) dx &= \int_\Omega \alpha_\varepsilon \left[|\Delta u_\varepsilon - \Delta u_0|^2 + 2\Delta u_0 \Delta(u_\varepsilon - u_0)\right] dx, \\ &= \int_\Omega \alpha_\varepsilon |\Delta(u_\varepsilon - u_0)|^2 dx + 2\int_\Omega \alpha_\varepsilon \Delta u_0 \Delta(u_\varepsilon - u_0) dx.\end{aligned}$$

Then, we get

$$\int_\Omega \alpha_\varepsilon |\Delta u_\varepsilon|^2 dx - \int_\Omega \alpha_0 |\Delta u_0|^2 dx = (\alpha_1 - \alpha_0) ab\pi\varepsilon^2 |\Delta u_0(0)|^2 + \int_\Omega \alpha_\varepsilon |\Delta(u_\varepsilon - u_0)|^2 dx + 2\int_\Omega \alpha_\varepsilon \Delta u_0 \Delta(u_\varepsilon - u_0) dx.$$

□

Lemma A.9. *We have*

$$\int_\Omega \beta_\varepsilon |\nabla u_\varepsilon|^2 dx - \int_\Omega \beta_0 |\nabla u_0|^2 dx = (\beta_1 - \beta_0) ab\pi\varepsilon^2 |\nabla u_0(0)|^2 + \int_\Omega \beta_\varepsilon |\nabla(u_\varepsilon - u_0)|^2 dx + 2\int_\Omega \beta_\varepsilon \nabla u_0 \nabla(u_\varepsilon - u_0) dx + o(\varepsilon^2).$$

Proof. We have

$$\begin{aligned}\int_\Omega \beta_\varepsilon|\nabla u_\varepsilon|^2dx-\int_\Omega \beta_0|\nabla u_0|^2dx &= \int_\Omega \beta_\varepsilon|\nabla u_\varepsilon|^2dx-\int_\Omega ((\beta_0-\beta_\varepsilon)+\beta_\varepsilon)|\nabla u_0|^2dx,\\ &= \int_\Omega \beta_\varepsilon\left(|\nabla u_\varepsilon|^2-|\nabla u_0|^2\right)dx-\int_{\omega_\varepsilon}(\beta_0-\beta_1)|\nabla u_0|^2dx,\\ &= (\beta_1-\beta_0)\left[\int_{\omega_\varepsilon}|\nabla u_0(x)|^2-|\nabla u_0(0)|^2dx+\int_{\omega_\varepsilon}|\nabla u_0(0)|^2dx\right]\\ &\quad+\int_\Omega \beta_\varepsilon|\nabla(u_\varepsilon-u_0)|^2dx+2\int_\Omega \beta_\varepsilon\nabla u_0\nabla(u_\varepsilon-u_0)dx.\end{aligned}$$

By using the variable, $\left(\frac{x_1}{a},\frac{x_2}{b}\right)=\varepsilon z$, and applying the Taylor formula to order 1 in the neighborhood of zero, we get the result. □

Let $X_\varepsilon=u_\varepsilon-u_0$, then it is easy to verify that X_ε is a solution of

$$\begin{cases}\Delta(\alpha_\varepsilon\Delta(X_\varepsilon))-\operatorname{div}(\beta_\varepsilon\nabla(X_\varepsilon))+R^*R(X_\varepsilon)+\mu X_\varepsilon=\Delta((\alpha_0-\alpha_\varepsilon)\Delta u_0)+\operatorname{div}((\beta_\varepsilon-\beta_0)\nabla u_0), & \text{in } \Omega,\\ \frac{\partial(\alpha_\varepsilon\Delta(X_\varepsilon))}{\partial n}-\beta_\varepsilon\frac{\partial(X_\varepsilon)}{\partial n}=\frac{\partial((\alpha_0-\alpha_\varepsilon)\Delta u_0)}{\partial n}+(\beta_\varepsilon-\beta_0)\frac{\partial u_0}{\partial n}, & \text{on } \partial\Omega,\\ \Delta(X_\varepsilon)=0, & \text{on } \partial\Omega.\end{cases}\tag{A7}$$

Using the same argument of the proof of (A5), we show that

$$||X_\varepsilon||_{H^2(\Omega)}=O(\varepsilon).\tag{A8}$$

Lemma A.10. *We have*

$$\int_{\omega_\varepsilon}\Delta((\alpha_\varepsilon-\alpha_0)\Delta u_0)X_\varepsilon dx=o(\varepsilon^2).$$

Proof. We have

$$\left|\int_{\omega_\varepsilon}\Delta((\alpha_\varepsilon-\alpha_0)\Delta u_0)X_\varepsilon dx\right|\le\|\Delta((\alpha_\varepsilon-\alpha_0)\Delta u_0)\|_{L^\infty(\omega_\varepsilon)}\int_{\omega_\varepsilon}|X_\varepsilon|dx.$$

By applying Hölder's inequality with $p,q\in[1,+\infty]$ such that $\frac{1}{p}+\frac{1}{q}=1$, we get

$$\begin{aligned}\left|\int_{\omega_\varepsilon}\Delta((\alpha_\varepsilon-\alpha_0)\Delta u_0)X_\varepsilon dx\right| &\le c\left(\int_{\omega_\varepsilon}1dx\right)^{\frac{1}{p}}\|X_\varepsilon\|_{L^q(\omega_\varepsilon)},\\ &\le c\left(\varepsilon^2ab\right)^{\frac{1}{p}}\|X_\varepsilon\|_{L^q(\omega_\varepsilon)}.\end{aligned}$$

By choosing $p=\frac{4}{3}$ and $q=4$ in the above and since the injection of $H^2(\Omega)$ in $L^4(\Omega)$ is continuous, we have

$$\left|\int_{\omega_\varepsilon}\Delta((\alpha_\varepsilon-\alpha_0)\Delta u_0)X_\varepsilon dx\right|\le c\left(\varepsilon^2ab\right)^{\frac{3}{4}}\|X_\varepsilon\|_{H^2(\Omega)}.$$

However,

$$\|X_\varepsilon\|_{H^2(\Omega)}=O(\varepsilon),$$

which gives

$$\left| \int_{\omega_\varepsilon} \Delta((\alpha_\varepsilon - \alpha_0)\Delta u_0)dx \right| \leq c\varepsilon^{\frac{5}{2}}(ab)^{\frac{3}{4}}$$

and finishes the proof of the lemma. □

Lemma A.11. *We have*

$$\int_{\omega_\varepsilon} \Delta u_0 X_\varepsilon dx = o(\varepsilon^2) \text{ and } \int_{\omega_\varepsilon} u_0 X_\varepsilon dx = o(\varepsilon^2).$$

Proof. We use the same approach as in the previous proof. □

Lemma A.12. *We have*

$$\int_\Omega \beta_\varepsilon |\nabla(u_\varepsilon - u_0)|^2 dx + \int_\Omega \alpha_\varepsilon |\Delta(u_\varepsilon - u_0)|^2 dx = o(\varepsilon^2).$$

Proof. Let $X_\varepsilon = u_\varepsilon - u_0$. By applying Green's formula, we show that

$$\begin{aligned}
&\int_\Omega \beta_\varepsilon |\nabla(X_\varepsilon)|^2 dx + \int_\Omega \alpha_\varepsilon |\Delta(X_\varepsilon)|^2 dx \\
&= -\int_\Omega \operatorname{div}(\beta_\varepsilon \nabla X_\varepsilon) X_\varepsilon dx + \int_{\partial\Omega} \beta_\varepsilon \frac{\partial X_\varepsilon}{\partial n} X_\varepsilon d\sigma - \int_\Omega \nabla(\alpha_\varepsilon \Delta(X_\varepsilon))\nabla X_\varepsilon dx + \int_{\partial\Omega} \alpha_\varepsilon \frac{\partial X_\varepsilon}{\partial n} \Delta X_\varepsilon d\sigma, \\
&= -\int_\Omega \operatorname{div}(\beta_\varepsilon \nabla X_\varepsilon) X_\varepsilon dx + \int_{\partial\Omega} \beta_\varepsilon \frac{\partial X_\varepsilon}{\partial n} X_\varepsilon d\sigma + \int_\Omega \Delta(\alpha_\varepsilon \Delta(X_\varepsilon)) X_\varepsilon dx - \int_{\partial\Omega} X_\varepsilon \frac{\partial(\alpha_\varepsilon \Delta X_\varepsilon)}{\partial n} d\sigma \\
&\quad + \int_{\partial\Omega} \alpha_\varepsilon \frac{\partial X_\varepsilon}{\partial n} \Delta X_\varepsilon d\sigma.
\end{aligned}$$

By multiplying (A7) by X_ε and integrating on Ω, we get

$$\begin{aligned}
&\int_\Omega \beta_\varepsilon |\nabla(X_\varepsilon)|^2 dx + \int_\Omega \alpha_\varepsilon |\Delta(X_\varepsilon)|^2 dx \\
&= -\int_\Omega |RX_\varepsilon|^2 dx + \int_\Omega \Delta((\alpha_0 - \alpha_\varepsilon)\Delta u_0) X_\varepsilon dx + \int_\Omega \operatorname{div}((\beta_\varepsilon - \beta_0)\nabla u_0) X_\varepsilon dx \\
&\quad - \mu \int_\Omega |X_\varepsilon|^2 dx + \int_{\partial\Omega} \frac{\partial((\alpha_\varepsilon - \alpha_0)\Delta u_0)}{\partial n} X_\varepsilon d\sigma + \int_{\partial\Omega} (\beta_0 - \beta_\varepsilon) \frac{\partial u_0}{\partial n} X_\varepsilon dx.
\end{aligned}$$

However, we have $\alpha_\varepsilon = \alpha_0$ (respectively, $\beta_\varepsilon = \beta_0$) on $\Omega \backslash \overline{\omega_\varepsilon}$, then according to the trace theorem, we deduce that $\alpha_\varepsilon = \alpha_0$ (respectively, $\beta_\varepsilon = \beta_0$) on $\partial\Omega$. Then, we have

$$\int_\Omega \beta_\varepsilon |\nabla(X_\varepsilon)|^2 dx + \int_\Omega \alpha_\varepsilon |\Delta(X_\varepsilon)|^2 dx \leq \int_\Omega \Delta((\alpha_0 - \alpha_\varepsilon)\Delta u_0) X_\varepsilon dx + \int_\Omega \operatorname{div}((\beta_\varepsilon - \beta_0)\nabla u_0) X_\varepsilon dx,$$

by resorting to Lemmas A.10 and A.11 which finishes the proof. □

APPENDIX B: TECHNICAL COMPUTATIONS FOR THE PROOF OF LEMMA A.5

We recall that E denotes the ellipse and $\mathbb{R}^2\backslash E$ the exterior domain. We denoted by $W^2(\mathbb{R}^2\backslash E)$ the weighted Sobolev space defined by

$$W^2(\mathbb{R}^2\backslash E)=\left\{u,\frac{u}{(1+r^2)\log(2+r^2)}\in L^2(\mathbb{R}^2\backslash E),\frac{\nabla u}{(1+r^2)^{\frac{1}{2}}\log(2+r^2)}\in L^2(\mathbb{R}^2\backslash E),\nabla^2 u\in L^2(\mathbb{R}^2\backslash E),\right\}$$

with $r=\|x\|$ and $W^2(\mathbb{R}^2\backslash E)/\wp_1$ the functional quotient space, where $\wp_1$ is the set of polynomial of degree less or equal than 1.

We assume that $H_\varepsilon=w_{\varepsilon|\Omega_\varepsilon}$ is the solution of the following problem:

$$\begin{cases}\alpha_0\Delta^2 H_\varepsilon-\beta_0\Delta H_\varepsilon+R^*RH_\varepsilon+\mu H_\varepsilon=0, & \text{in } \Omega_\varepsilon,\\ \alpha_0\frac{\partial(\Delta H_\varepsilon)}{\partial n}-\beta_0\frac{\partial H_\varepsilon}{\partial n}=g_\varepsilon(0), & \text{on } \partial\Omega,\\ \Delta H_\varepsilon=0, & \text{on } \partial\Omega,\\ \alpha_0\frac{\partial(\Delta H_\varepsilon)}{\partial n}-\beta_0\frac{\partial H_\varepsilon}{\partial n}=-\alpha_0\frac{\partial(\Delta u_0)}{\partial n}+\beta_0\frac{\partial(u_0)}{\partial n}, & \text{on } \partial\omega_\varepsilon,\\ \Delta H_\varepsilon=-\Delta v_0, & \text{on } \partial\omega_\varepsilon.\end{cases}\tag{B1}$$

By splitting H_ε as $H_\varepsilon=\varepsilon^2 T\left(\frac{x}{\varepsilon}\right)+e_\varepsilon$, we show that $T_\varepsilon\in W^2(\mathbb{R}^2\backslash E)/\wp_1$ solution for the exterior problem:

$$\begin{cases}\Delta^2 T=0, & \text{in } \mathbb{R}^2\backslash E,\\ \alpha_0\frac{\partial\Delta T}{\partial n}=0, & \text{on } \partial E,\\ \Delta T=-\Delta v_0(0), & \text{on } \partial E,\end{cases}\tag{B2}$$

and e_ε is the solution of the following problem:

$$\begin{cases}\alpha_0\Delta^2 e_\varepsilon-\beta_0\Delta e_\varepsilon+R^*Re_\varepsilon+\mu e_\varepsilon=F_\varepsilon & \text{in } \Omega_\varepsilon,\\ \alpha_0\frac{\partial\Delta e_\varepsilon}{\partial n}-\beta_0\frac{\partial e_\varepsilon}{\partial n}=-\frac{\alpha_0}{\varepsilon}\frac{\partial T\left(\frac{x}{\varepsilon}\right)}{\partial n}+\beta_0\varepsilon\frac{\partial T\left(\frac{x}{\varepsilon}\right)}{\partial n}+g_\varepsilon(0) & \text{on } \partial\Omega,\\ \Delta e_\varepsilon=-\Delta\left(T\left(\frac{x}{\varepsilon}\right)\right) & \text{on } \partial\Omega,\\ \alpha_0\frac{\partial\Delta e_\varepsilon}{\partial n}-\beta_0\frac{\partial e_\varepsilon}{\partial n}=-\alpha_0\left(\frac{1}{\varepsilon}\frac{\partial T\left(\frac{x}{\varepsilon}\right)}{\partial n}+\frac{\partial(\Delta u_0)}{\partial n}\right)+\beta_0\left(\varepsilon\frac{\partial T\left(\frac{x}{\varepsilon}\right)}{\partial n}+\frac{\partial u_0}{\partial n}\right) & \text{on } \partial\omega_\varepsilon,\\ \Delta e_\varepsilon=-\left(\Delta v_0-\Delta v_0(0)\right) & \text{on } \partial\omega_\varepsilon,\end{cases}\tag{B3}$$

with $F_\varepsilon=\beta_0\Delta T\left(\frac{x}{\varepsilon}\right)-\varepsilon^2R^*RT\left(\frac{x}{\varepsilon}\right)-\mu\varepsilon^2T\left(\frac{x}{\varepsilon}\right)$.

Lemma B.1. *We have*

$$\int_{\partial\omega_\varepsilon}w_\varepsilon\frac{\partial\Delta u_0}{\partial n}dx=o(\varepsilon^2).$$

Proof. According to Lemma B.6 in Aubert and Drogoul,[30] we have

$$\|w_\varepsilon\|_{0,\Omega_\varepsilon}=O(-\varepsilon^2\log(\varepsilon)).$$

Using the Cauchy–Schwartz inequality and the trace theorem, we show that

$$\left|\int_{\partial\omega_\varepsilon}w_\varepsilon\frac{\partial\Delta u_0}{\partial n}dx\right|\leqslant\|w_\varepsilon\|_{0,\Omega_\varepsilon}\left(\int_{\partial\omega_\varepsilon}|\Delta u_0|^2d\sigma\right)^{\frac{1}{2}}.$$

By taking the change of variable $\left(\frac{x_1}{\epsilon}, \frac{x_2}{\epsilon}\right) = \epsilon z$, we obtain

$$\left(\int_{\partial\omega_\epsilon} |\Delta u_0|^2 d\sigma\right)^{\frac{1}{2}} = O\left(\sqrt{\epsilon}\right).$$

Then, we deduce

$$\int_{\partial\omega_\epsilon} w_\epsilon \frac{\partial \Delta u_0}{\partial n} dx = o(\epsilon^2).$$

□

From Theorem B.3 in Aubert and Drogoul,[30] the authors show that the following exterior problem:

$$(\mathcal{P}_{ext}) \begin{cases} \Delta^2 T = 0, & \text{in } \mathbb{R}^2 \backslash E, \\ \frac{\partial \Delta T}{\partial n} = g_1, & \text{on } \partial E, \\ \Delta T = g_2, & \text{on } \partial E, \end{cases} \tag{B4}$$

where $g_1 \in H^{-\frac{3}{2}}(\partial E)$ and $g_2 \in H^{-\frac{1}{2}}(\partial E)$ admits a unique solution $T \in W^2(\mathbb{R}^2 \backslash E)/\wp_1$, given by

$$T(x) = \int_{\partial E} \lambda_1(y) E(x-y) d\sigma(y) + \int_{\partial B} \lambda_2(y) \partial_{n_y} E(x-y) d\sigma(y), \forall x \in \mathbb{R}^2 \backslash E,$$

where $E(x-y) = -\frac{1}{8\pi}\|x-y\|^2 \log(\|x-y\|)$ and λ_1, λ_2 satisfy:

$$\begin{aligned}
&-\frac{\lambda_1(x)}{2} + \int_{\partial E} \lambda_1(y) \partial_{n_x}(\Delta E(x-y)) d\sigma(y) + \oint_{\partial E} \lambda_2(y) \partial_{n_x}(\Delta(\partial_{n_y} E(x-y))) d\sigma(y) + a_0 + a_1 x + a_2 x_2 = g_1(x) \\
&\frac{\lambda_2(x)}{2} + \int_{\partial E} \lambda_1(y) \Delta_x(E(x-y)) d\sigma(y) + \int_{\partial E} \lambda_2(y) \Delta_x(\partial_{n_y} E(x-y)) d\sigma(y) - a_1 n_1(x) - a_2 n_2(x) = g_2(x) \\
&\langle \lambda_1, 1 \rangle = 0, \\
&\langle \lambda_1, x_1 \rangle + \langle \lambda_2, n_1 \rangle = 0, \\
&\langle \lambda_1, x_2 \rangle + \langle \lambda_2, n_2 \rangle = 0,
\end{aligned}$$

where $x = (x_1, x_2) \in \partial E$, $n = (n_1, n_2)$, $\oint$ denotes the principal Cauchy value and $a_1, a_2, a_3 \in \mathbb{R}$. Moreover, the jump relation across ∂E is the following:

$$\begin{aligned}
g_1(x) - \partial_n(\Delta(L^T))(x) &= -\lambda_1(x), \\
g_2(x) - \Delta(L^T)(x) &= \lambda_2(x),
\end{aligned}$$

where L^T is the solution of the following problem:

$$\begin{cases} \Delta^2 L^T = 0, & \text{in } E, \\ \partial_n L^T = \partial_n T, & \text{on } \partial E, \\ L^T = T, & \text{on } \partial E. \end{cases} \tag{B5}$$

By setting $x = (a\cos(\varphi), b\sin(\varphi))$ and $y = (a\cos(\theta), b\sin(\theta))$ and using the same computation technique of λ_1 and λ_2 in Aubert and Drogoul[30], (pp18–20), with $g_1 = 0$ and $g_2 = -\Delta v_0(0)$, we show that

$$\begin{aligned}
&\Delta_x(E(x-y)) = -\frac{2}{8\pi}(\log(2(1-\cos(\varphi-\theta))),\\
&\Delta_x(\partial_{n_y}E(x-y)) = \frac{-1}{4\pi},\\
&\partial_{n_x}(\Delta E(x-y)) = \frac{-1}{4\pi},\\
&\partial_{n_x}\Delta(\partial_{n_y}(E(x-y)) = \frac{2}{8\pi(1-\cos(\varphi-\theta))},\\
&a_0 = a_1 = a_2 = 0,\\
&\lambda_1 = 0 \text{ and } \lambda_2 = k_0^{a,b}\Delta v_0(0) \qquad \text{(see details below)},\\
&\oint_{\partial E}\partial_{n_x}(\Delta(\partial_{n_y}E(x-y)))d\sigma(y) = 0.
\end{aligned}$$

We have λ_2 satisfies

$$\frac{\lambda_2}{2} + \int_{\partial E}\lambda_2\Delta_x(\partial_{n_y}E(x-y))d\sigma(y) = -\Delta v_0(0),$$

from which we deduce

$$\frac{\lambda_2}{2} - \frac{\lambda_2}{4\pi}\int_{\partial E}d\sigma(y) = -\Delta v_0(0).$$

So if $a \neq b$, we obtain

$$\lambda_2 = k_0^{a,b}\Delta v_0(0),$$

where

$$k_0^{a,b} = \frac{2\pi}{\frac{1}{2}\int_0^{2\pi}\sqrt{a^2\cos^2(\theta)+b^2\sin^2(\theta)}d\theta - \pi}.$$

Lemma B.2. *We have*

$$\int_{\partial\omega_\epsilon}\partial_n w_\epsilon\Delta u_0 d\sigma(x) = -\epsilon^2(k_0^{a,b}+1)\Delta v_0(0)\left(k_1^{a,b}\frac{\partial^2u_0(0)}{\partial x^2} + k_2^{a,b}\frac{\partial^2u_0(0)}{\partial y^2} + k_3^{a,b}\left(\frac{\partial^2u_0(0)}{\partial x\partial y} + \frac{\partial^2u_0(0)}{\partial y\partial x}\right)\right) + o(\epsilon^2),$$

where

$$\begin{aligned}
k_0^{a,b} &= \frac{2\pi}{\frac{1}{2}\int_0^{2\pi}\sqrt{a^2\cos^2(\theta)+b^2\sin^2(\theta)}d\theta - \pi},\\
k_1^{a,b} &= \int_0^{2\pi}\frac{a^2\cos^2(\theta)}{\sqrt{a^2\cos^2(\theta)+b^2\sin^2(\theta)}}d\theta,\\
k_2^{a,b} &= \int_0^{2\pi}\frac{b^2\sin^2(\theta)}{\sqrt{a^2\cos^2(\theta)+b^2\sin^2(\theta)}}d\theta,\\
k_3^{a,b} &= \int_0^{2\pi}\frac{ab\cos(\theta)\sin(\theta)}{\sqrt{a^2\cos^2(\theta)+b^2\sin^2(\theta)}}d\theta.
\end{aligned}$$

Proof. We have

$$\int_{\partial\omega_\varepsilon} \partial_n w_\varepsilon \Delta u_0 d\sigma(x) = \int_{\partial\omega_\varepsilon} \partial_n H_\varepsilon \Delta u_0 d\sigma(x), = \int_{\partial\omega_\varepsilon} \partial_n \varepsilon^2 T\left(\frac{x}{\varepsilon}\right) \Delta u_0 d\sigma(x) + \int_{\partial\omega_\varepsilon} \partial_n e_\varepsilon \Delta u_0 d\sigma(x),$$

By using classical calculation techniques, as it is done in Lemma B.1, we show

$$\int_{\partial\omega_\varepsilon} \partial_n e_\varepsilon \Delta u_0 d\sigma(x) = o(\varepsilon^2).$$

Then, we deduce

$$\int_{\partial\omega_\varepsilon} \partial_n w_\varepsilon \Delta u_0 d\sigma(x) = \int_{\partial\omega_\varepsilon} \partial_n \varepsilon^2 T\left(\frac{x}{\varepsilon}\right) \Delta u_0 d\sigma(x) + o(\varepsilon^2).$$

By writing $\tilde{u}_0(x) = u_0(x) - u_0(0) - \nabla u_0(0)$, we get

$$\int_{\partial\omega_\varepsilon} \partial_n \varepsilon^2 T\left(\frac{x}{\varepsilon}\right) \Delta u_0 d\sigma(x) = \int_{\partial\omega_\varepsilon} \partial_n \varepsilon^2 T\left(\frac{x}{\varepsilon}\right) \Delta \tilde{u}_0 d\sigma(x).$$

By applying Green's formula, we obtain

$$\int_{\partial\omega_\varepsilon} \partial_n \varepsilon^2 T\left(\frac{x}{\varepsilon}\right) \Delta u_0 d\sigma(x) = \int_{\omega_\varepsilon} \Delta\left(\varepsilon^2 T\left(\frac{x}{\varepsilon}\right)\right) \Delta(\tilde{u_0}) dx + \int_{\omega_\varepsilon} \nabla\left(\varepsilon^2 T\left(\frac{x}{\varepsilon}\right)\right) \nabla(\Delta(\tilde{u_0})) dx.$$

By using classical calculation techniques, as it is done in Lemma A.4, we show

$$\int_{\omega_\varepsilon} \nabla\left(\varepsilon^2 T\left(\frac{x}{\varepsilon}\right)\right) \nabla(\Delta(\tilde{u_0})) dx = o(\varepsilon^2).$$

Then, we deduce

$$\int_{\partial\omega_\varepsilon} \partial_n \varepsilon^2 T\left(\frac{x}{\varepsilon}\right) \Delta u_0 d\sigma(x) = \int_{\omega_\varepsilon} \Delta\left(\varepsilon^2 T\left(\frac{x}{\varepsilon}\right)\right) \Delta(\tilde{u_0}) dx + o(\varepsilon^2).$$

By applying Green's formula, we obtain

$$\int_{\omega_\varepsilon} \Delta\left(\varepsilon^2 T\left(\frac{x}{\varepsilon}\right)\right) \Delta(\tilde{u_0}) dx = \int_{\omega_\varepsilon} \underbrace{\Delta^2\left(\varepsilon^2 T\left(\frac{x}{\varepsilon}\right)\right)}_{=0} \tilde{u_0} dx + \int_{\partial\omega_\varepsilon} \left[\partial_n \tilde{u_0} \Delta\left(\varepsilon^2 T\left(\frac{x}{\varepsilon}\right)\right) - \partial_n\left[\Delta\left(\varepsilon^2 T\left(\frac{x}{\varepsilon}\right)\right)\right] \tilde{u_0}\right] d\sigma.$$

By using the change of variable $x = \varepsilon y$, we obtain

$$\begin{aligned}\int_{\omega_\varepsilon}\Delta\left(\varepsilon^2 T\left(\frac{x}{\varepsilon}\right)\right)\Delta(\tilde{u_0})dx &= \varepsilon\int_{\partial E}\Delta\left(L^T(y)\right)\partial_n\tilde{u_0}(\varepsilon y)d\sigma(y) - \int_{\partial E}\partial_n\left(\Delta(L^T)\right)\tilde{u_0}(\varepsilon y)d\sigma(y)\\ &= \varepsilon\int_{\partial E}\Delta\left(L^T(y)\right)\underbrace{\left(\partial_n\tilde{u_0}(\varepsilon y) - \varepsilon\nabla^2 u_0(0)y\cdot n\right)}_{=o(\varepsilon)}d\sigma(y) + \varepsilon^2\int_{\partial E}\Delta\left(L^T(y)\right)\nabla^2 u_0(0)y\cdot n d\sigma(y)\\ &\quad - \int_{\partial E}\partial_n\left(\Delta(L^T)\right)\underbrace{\left(\tilde{u_0}(\varepsilon y) - \frac{\varepsilon^2}{2}\nabla^2 u_0(0)y\cdot y\right)}_{=o(\varepsilon^2)}d\sigma(y) - \frac{\varepsilon^2}{2}\int_{\partial E}\partial_n\left(\Delta(L^T)\right)\nabla^2 u_0(0)y\cdot y d\sigma(y)\\ &= \varepsilon^2\int_{\partial E}\Delta\left(L^T(y)\right)\nabla^2 u_0(0)y\cdot n d\sigma(y) - \frac{\varepsilon^2}{2}\int_{\partial E}\partial_n\left(\Delta(L^T)\right)\nabla^2 u_0(0)y\cdot y d\sigma(y) + o(\varepsilon^2).\end{aligned}$$

According to the jump relation across ∂E and the values of λ_1, λ_2, g_2, and g_1, we deduce

$$\begin{aligned}\int_{\omega_\varepsilon}\Delta\left(\varepsilon^2 T\left(\frac{x}{\varepsilon}\right)\right)\Delta(\tilde{u_0})dx &= \varepsilon^2\int_{\partial E}(-\lambda_2 + g_2(y))\nabla^2 u_0(0)y\cdot n d\sigma(y) + o(\varepsilon^2),\\ &= -\varepsilon^2\left(k_0^{a,b}+1\right)\Delta v_0(0)\int_{\partial E}\frac{\nabla^2 u_0(0)y\cdot y}{\|y\|}d\sigma(y) + o(\varepsilon^2).\end{aligned}$$

By setting $y = (a\cos(\theta), b\sin(\theta))$, we show that

$$\nabla^2 u_0(0)y\cdot y = a^2\cos^2(\theta)\frac{\partial^2 u_0(0)}{\partial x^2} + ab\cos(\theta)\sin(\theta)\frac{\partial^2 u_0(0)}{\partial x\partial y} + ab\cos(\theta)\sin(\theta)\frac{\partial^2 u_0(0)}{\partial y\partial x} + b^2\sin^2(\theta)\frac{\partial^2 u_0(0)}{\partial y^2}.$$

Then, we deduce that

$$\int_{\omega_\varepsilon}\Delta\left(\varepsilon^2 T\left(\frac{x}{\varepsilon}\right)\right)\Delta(\tilde{u_0})dx = -\varepsilon^2(k_0^{a,b}+1)\Delta v_0(0)\left(k_1^{a,b}\frac{\partial^2 u_0(0)}{\partial x^2} + k_2^{a,b}\frac{\partial^2 u_0(0)}{\partial y^2} + k_3^{a,b}\left(\frac{\partial^2 u_0(0)}{\partial x\partial y} + \frac{\partial^2 u_0(0)}{\partial y\partial x}\right)\right) + o(\varepsilon^2),$$

where

$$\begin{aligned}k_0^{a,b} &= \frac{2\pi}{\frac{1}{2}\int_0^{2\pi}\sqrt{a^2\cos^2(\theta)+b^2\sin^2(\theta)}d\theta - \pi},\\ k_1^{a,b} &= \int_0^{2\pi}\frac{a^2\cos^2(\theta)}{\sqrt{a^2\cos^2(\theta)+b^2\sin^2(\theta)}}d\theta,\\ k_2^{a,b} &= \int_0^{2\pi}\frac{b^2\sin^2(\theta)}{\sqrt{a^2\cos^2(\theta)+b^2\sin^2(\theta)}}d\theta,\\ k_3^{a,b} &= \int_0^{2\pi}\frac{ab\cos(\theta)\sin(\theta)}{\sqrt{a^2\cos^2(\theta)+b^2\sin^2(\theta)}}d\theta.\end{aligned}$$

Then, we deduce that

$$\int_{\partial\omega_\varepsilon}\partial_n\varepsilon^2 T\left(\frac{x}{\varepsilon}\right)\Delta u_0 d\sigma(x) = -\varepsilon^2(k_0^{a,b}+1)\Delta v_0(0)\left(k_1^{a,b}\frac{\partial^2 u_0(0)}{\partial x^2} + k_2^{a,b}\frac{\partial^2 u_0(0)}{\partial y^2} + k_3^{a,b}\left(\frac{\partial^2 u_0(0)}{\partial x\partial y} + \frac{\partial^2 u_0(0)}{\partial y\partial x}\right)\right) + o(\varepsilon^2).$$

□